Zoological Journal of the Linnean Society, 2025, **204**, zlaf048
https://doi.org/10.1093/zoolinnean/zlaf048
Advance access publication 8 July 2025
Original Article

OXFORD

Original Article

An unexpectedly diverse new genus of catfishes (Siluriformes, Heptapteridae) endemic to the Magdalena River basin, Colombia

Carlos DoNascimiento[1,*], Francisco Antonio Villa-Navarro[2], Juan G. Albornoz-Garzón[3], Cristhian C. Conde-Saldaña[4], Gabriel S.C. Silva[5], Alejandro Méndez-López[6], Fábio F. Roxo[5], Armando Ortega-Lara[7], Claudio Oliveira[5]

[1]Grupo de Ictiología, Instituto de Biología, Facultad de Ciencias Exactas y Naturales, Universidad de Antioquia, Medellín, 050010, Colombia
[2]Grupo de Investigación en Zoología, Facultad de Ciencias, Universidad del Tolima, Ibagué, 730006, Colombia
[3]Department of Ecology and Evolutionary Biology, University of Michigan, Ann Arbor, MI 48109, United States
[4]Division of Fishes, Department of Vertebrate Zoology, National Museum of Natural History, Smithsonian Institution, Washington, DC 20560, United States
[5]Instituto de Biociências, Universidade Estadual Paulista Júlio de Mesquita Filho, Botucatu, São Paulo, 18618-689, Brazil
[6]Fundación Miguel Lillo, Unidad Ejecutora Lillo (UEL-CONICET), San Miguel de Tucumán, T4000JFE, Argentina
[7]Grupo de Investigación en Peces Neotropicales, Fundación para la Investigación y el Desarrollo Sostenible FUNINDES, Cali, 760035, Colombia

[*]Corresponding author. Grupo de Ictiología, Instituto de Biología, Facultad de Ciencias Exactas y Naturales, Universidad de Antioquia, Medellín, Colombia. E-mail: c.donascimiento@udea.edu.co

ABSTRACT

A new genus of heptapterid catfish, ***Magdalenichthys* gen. nov.**, largely ignored for the past two decades is herein described. Comprehensive examination of specimens in Colombian ichthyological collections and additional samplings in the Magdalena basin were the base for an integral analysis using morphological characters, DNA barcode delimitation, and molecular phylogenetic analyses to assess monophyly and relationships of the new genus, and to delimit and diagnose four new species, ***Magdalenichthys lundbergi*** sp. nov., ***Magdalenichthys mompox*** sp. nov., ***Magdalenichthys poira*** sp. nov., and ***Magdalenichthys yariguies*** sp. nov., endemic to the Magdalena basin. The new genus is phylogenetically diagnosed. Maximum likelihood, Bayesian inference, and coalescent-based analyses with ultraconserved elements (UCEs) data, place the new genus as sister to *Phenacorhamdia*, within a clade also containing *Cetopsorhamdia* and *Pariolius*, consistent with the finding of two apomorphic characters shared by the new genus and *Phenacorhamdia*. The biogeographic pattern of the new genus (restricted to the Magdalena basin) is also discussed.

Keywords: Andes; DNA barcode; freshwater fishes; iterative taxonomy; phylogenomics; South America; species delimitation; systematics; trans-Andean; ultraconserved elements

INTRODUCTION

The family Heptapteridae is a conspicuous and ubiquitous group of small-sized Neotropical catfishes (most species are less than 20 cm standard length -SL), comprising 237 valid species and more than 50 recognized undescribed forms (Reis *et al.* 2003, Fricke *et al.* 2024). Members of the family are distributed from northern Mexico to southern Argentina, on both sides of the Andes, being one of the most characteristic components of the ichthyofaunas of small body waters in the Neotropics (Bockmann and Guazelli 2003).

The monophyly of the family was first recognized by Lundberg and McDade (1986) and formalized as a taxon at the subfamily level within Pimelodidae (Rhamdiinae = Heptapterinae, see Silfvergrip 1996, on nomenclatural priority

Received 12 July 2024; revised 11 March 2025; accepted 17 April 2025
[Version of Record, first published online 8 July 2025, with fixed content and layout in compliance with Art. 8.1.3.2 ICZN. http://zoobank.org/urn:lsid:zoobank.org:pub:09F32436-D4F8-4F1F-A134-9A585C1C586B]

of the latter) by Lundberg *et al.* (1991). Preliminary phylogenetic analyses dealing with the whole Siluriformes (Mo 1991, de Pinna 1993) suggested that heptapterids do not comprise a monophyletic clade exclusively with the remaining subfamilies of the former Pimelodidae (i.e. Pimelodinae and Pseudopimelodinae), but instead heptapterids are allied to a suprafamilial clade constituted by Ariidae, Auchenipteridae, Doradidae, Mochokidae, and Pimelodidae, or it is recovered as sister to the Asian Bagrichthyidae (= Bagridae), respectively. Bockmann (1998) discussed some morphological evidence that refuted de Pinna's hypothesis (i.e. non-monophyly of Bagridae *sensu* Mo 1991, and monophyly of his Rhamdioidei = Heptapt eridae + Bagrichthyidae + Olyridae), suggesting a sister group relationship of Heptapteridae to a large clade composed by Ariidae, Auchenipteridae, Austroglanididae, Bagridae, Chacidae, Claroteidae, Cranoglanididae, Doradidae, Horabagridae, Ictaluridae, Malapteruridae, Mochokidae, Pangasiidae, Plotosidae, Pimelodidae, Schilbidae, and Siluridae. Bockmann and Guazelli (2003) taking into account the previous evidence of non-monophyly of the traditional notion of Pimelodidae (i.e. comprising subfamilies Heptapterinae, Pimelodinae, and Pseudopimelodinae), formally ranked the Rhamdiinae concept of Lundberg *et al.* (1991) at full family status level as Heptapteridae. In spite of previous morphological evidence suggesting non-monophyly of the whole Pimelodidae (i.e. Heptap terinae + Pimelodinae + Pseudopimelodinae), Diogo (2005, 2007) proposed four putative morphological synapomorphies for the classical Pimelodidae, associated with the mandibular barbels and cranial muscles. This hypothesis has gained support from molecular analyses as well (Hardman 2005, Sullivan *et al.* 2006, 2013, Silva *et al.* 2024) and seems acceptable today, given the growing support from multiple molecular datasets tested (Betancur-R *et al.* 2017) and combined analyses of multilocus DNA sequences with morphological characters (Mirande 2017). Currently, the original concept of Pimelodidae has been ranked as superfamily Pimelodoidea (Sullivan *et al.* 2006, 2013).

Heptapteridae monophyly has remained unchallenged and the group is diagnosed by the following synapomorphies that were proposed since its early recognition as a monophyletic group (Lundberg and McDade 1986, Ferraris 1988, Lundberg *et al.* 1991): (i) posterior arm of fourth transverse process laterally expanded above swimbladder and notched once to several times; (ii) neural spines of the Weberian complex centrum joined by a straight-edged, horizontal or sometimes a sloping bony lamina; (iii) process for insertion of levator operculi muscle on posterodorsal corner of hyomandibula greatly expanded; (iv) posterior and anterior limbs of quadrate articulating independently with hyomandibula and metapterygoid, respectively; (v) presence of an anteriorly recurved process ('mesethmoid hook'), projected from ventrolateral corner of mesethmoid. Regarding its internal relationships, a large monophyletic unit within the family, comprising the majority of genera characterized by lacking a free orbital rim was also recognized early (Lundberg and McDade 1986, Stewart 1986) and was informally denominated as the *Nemuroglanis* sub-clade by Ferraris (1988), who proposed the following derived conditions supporting its monophyly: (i) laminar portion of complex centrum transverse process (posterior to branched segment), triangular and extending nearly to the lateral tip of the fifth vertebral transverse process; (ii) first dorsal-fin pterygiophore inserted posterior to the Weberian complex, usually between vertebrae 7 and 10; (iii) dorsal-fin spine thin and flexible and spinelet (= first dorsal spine) absent; (iv) distal half of pectoral-fin spine thin and flexible. Bockmann (1994) proposed 11 additional synapomorphies for the *Nemuroglanis* subclade. The most comprehensive study dealing with the whole family is still the unpublished doctoral dissertation of Bockmann (1998), which gives a detailed revision of all genera included in the group and their relationships. More recently, two papers dealing with the internal relationships of Heptapteridae (although differing in their taxonomic coverage emphasis), based on molecular information (either traditional multi-locus and genomic data) were almost simultaneously published (Faustino-Fuster *et al.* 2021: multi-locus, Silva *et al.* 2021: ultraconserved elements). Interestingly, both contributions arrived at basically equivalent classification proposals (only differing in assignation of the monotypic *Goeldiella* to its separate tribe, Goeldiellini, by Faustino-Fuster *et al.* 2021), which in general terms also agree with previous findings earlier provided by Bockmann (1998). However, Faustino-Fuster *et al.* (2021) and Silva *et al.* (2021) significantly depart from each other in their approach to diagnose the recognized suprageneric clades, since only the latter provide strictly phylogenetic diagnoses for the groups being named. The former *Nemuroglanis* sub-clade was then formally ranked as tribe Heptapterini in both works, being diagnosed by 12 synapomorphies in Silva *et al.* (2021), which were mostly compiled from Bockmann (1994, 1998). In contrast, resolution at the genus level is far from being settled. With a few exceptions, e.g. *Cetopsorhamdia* Eigenmann & Fisher, 1916 (Bockmann and Reis 2021), *Gladioglanis* Ferraris & Mago-Leccia, 1989 (Lundberg *et al.* 1991), *Horiomyzon* Stewart, 1986 (Stewart 1986), *Mastiglanis* Bockmann, 1994 (Bockmann 1994), *Nemuroglanis* Eigenmann & Eigenmann, 1889 (Bockmann and Ferraris 2005), *Rhamdella* Eigenmann & Eigenmann, 1888 (Bockmann and Miquelarena 2008), and *Rhamdiopsis* Haseman, 1911 (Bockmann and Castro 2010), the bulk of remaining heptapterid genera lack of unambiguous diagnoses formulated in the context of a cladistic framework. This scenario renders in an unstable generic classification of an important number of species formerly described in the Heptapterini genera *Cetopsorhamdia*, *Chasmocranus*, Eigenmann, 1912, *Heptapterus* Bleeker, 1858, and *Imparfinis* Eigenmann & Norris, 1900.

Since 2006, a species then alternatively assigned to *Imparales panamensis* Bussing, 1970, *Heptapterus* sp., or even just as an undetermined Heptapteridae has been recorded for the upper basin of the Magdalena River in Colombia (Villa-Navarro *et al.* 2006, Albornoz-Garzón *et al.* 2020) and its systematic and taxonomic status have remained unexplored. A comprehensive revision of heptapterid material available in Colombian collections, as well as recent sampling efforts conducted along the Cauca and Magdalena rivers have allowed the recognition of three additional related forms, using an integrative approach. All these samples span a vast distribution area along the entire Magdalena basin. Encompassing morphological comparisons across heptapterids revealed the consistent presence of an exclusive derived character shared by these four species that provides support for its recognition as a monophyletic group within the family. In the present paper we propose a new genus to accommodate these four new species, which are recognized both by morphological

characters and DNA barcode delimitation analyses. Also, phylogenetic relationships of the new genus are addressed through its inclusion in the dataset of the recent phylogenetic assessment of Heptapteridae by Silva *et al.* (2021), based on high-throughput sequencing of ultraconserved elements (UCEs; Faircloth *et al.* 2012), complemented by a morphological comparative evaluation focussed on those characters that support its phylogenetic placement recovered in the molecular hypothesis.

MATERIAL AND METHODS

Morphology

Measurements were taken on the left side of specimens, whenever was possible, using a pointed tip digital caliper and expressed to the nearest 0.1 mm. Methodology and terminology for measurements followed Bockmann and de Pinna (2004). Caudal-fin ray counts followed Lundberg and Baskin (1969). Nomenclature for osteology and sensory pores of cephalic lateral line followed Bockmann and Miquelarena (2008). Number of branchiostegal rays, vertebrae, ribs, pterygiophores, procurrent (unsegmented) rays in anal and caudal fins, insertion of first and last pterygiophores of dorsal and anal fins, and other osteological characters were determined only on cleared and stained specimens. Vertebral counts include first five vertebrae involved in the Weberian complex and the compound caudal centrum consisting of preural centrum 1 and ural centrum 1 ($PU_1 + U_1$) was counted as one element (Lundberg and Baskin 1969). Thoracic vertebrae are here defined as the anteriormost precaudal vertebrae lacking a complete hemal arch. Counts of the holotype are indicated by an asterisk or enclosed in parenthesis. Cleared and stained specimens (c&s) were obtained using the Taylor and Van Dyke (1985) technique. Photographs of anatomical structures were taken with a Leica MC 190 HD digital camera attached to a Leica S8APO stereomicroscope, using the Leica Application Suite v.3.3.0. Final edited figures were composite multifocal images of individual photographs stacked using Helicon Focus v.6.7.1 Pro software. Institutional abbreviations follow Sabaj (2023).

DNA barcode species delimitation

Species delimitation analyses included 19 specimens of the new genus plus *Heptapterus longicauda* (Borodin, 1927) as an outgroup. Supporting information, Table S1 contains voucher information and BOLD accession numbers. Genomic DNA was extracted from muscle or fins tissues preserved in 95% ethanol with a Qiagen DNeasy Blood & Tissue kit, according to the manufacturer's instructions. Partial sequences of the mitochondrial gene cytochrome oxidase *c* subunit I (*COI*) were amplified using one round of PCR using the primers Fish F1 and Fish R1 (Ward *et al.* 2005). The PCR reactions were carried out in a reaction volume of 12.5 µl containing: 8.15 µl of H_2O, 1.25 µl of 10 × Taq buffer (500 mM KCl; 200 mM Tris-HCl), 0.4 µl of $MgCl_2$ (50 mM), 0.5 µl of dNTPs (8 mM), 0.25 µl of each primer (10 µM), 0.2 µl (5 U/µl) of Taq polymerase (Phoneutria®), and 1.5 µl of template DNA (50 ng/µl). The PCR conditions consisted of 3 min at 95°C (initial denaturation) followed by 35 cycles of 45 s at 94°C (denaturation), 30 s at 50–54°C (hybridization), and 60 s at 68°C (nucleotide extension), ending with a final extension at 68°C for 10 minutes. Amplified products were checked on a 1% agarose gel. Amplicons were then purified with ExoSAP-IT (USB Corporation) following the manufacturer's protocol. The purified products were used as a template to sequence both DNA strands using the BigDye Terminator v.3.1 Cycle Sequencing Ready Reaction kit (Applied Biosystems) and sequenced on an ABI3130 Genetic Analyzer (Applied Biosystems). Consensus sequences were assembled and edited in Geneious 4.8.5 (Kearse *et al.* 2012), and were aligned using Muscle algorithm (Edgar 2004), coupled to Geneious 4.8.5. The aligned matrix was tested for saturation in DAMBE v.7.0.28 (Xia 2018).

Species delimitation approaches involved three methods: (i) the general mixed Yule coalescent (GMYC; Fujisawa and Barraclough 2013), using the single threshold parameter at the web server (https://species.h-its.org/gmyc/), and as input an ultrametric gene tree. BEAST v.1.8 (Drummond *et al.* 2012) was used to estimate the ultrametric gene tree under the exponential growth coalescent model (Griffiths and Tavaré 1994) and the lognormal relaxed clock model (Drummond *et al.* 2006). The nucleotide evolutionary model used to estimate the ultrametric tree was the general time reversible model of rate substitution and gamma-distributed rates among sites (GTR+G), as estimated by PartitionFinder v.1.1.0 (Lanfear *et al.* 2012). Markov chains included a total of 1000 million generations, sampling trees every 100 000 generations. The convergence of the values was checked in Tracer v.1.6 (Rambaut *et al.* 2014). The first 10% generations were discarded as burn-in and the remaining trees were used to build a majority consensus tree in TreeAnnotator v.1.8 (Drummond *et al.* 2012). (ii) The Bayesian Poisson Tree Process (PTP; Zhang *et al.* 2013) was performed at the PTP webserver (https://species.h-its.org/), using 100 000 generations (thinning = 100) and a best maximum likelihood (ML) tree as input, obtained through an ML analysis. The ML analysis was performed with RaxML v.8.2 (Stamatakis 2014) with the GTR-GAMMA model, a maximum parsimony starting tree, and *a posteriori* analysis of bootstrap with the autoMRE function (Pattengale *et al.* 2009). (iii) The ASAP analysis was performed on the ASAP server (https://bioinfo.mnhn.fr/abi/public/asap/) using the Kimura (K80) model and only considered the partition with the lower ASAP-score.

Sequences were binned into species groups aimed to apply the genetic distances approach. Genetic distances were calculated using the Tamura-Nei (TN93) model (Tamura and Nei 1993) and 1000 bootstrap replicates in MEGA X (Kumar *et al.* 2018).

Phylogenomic analyses

The phylogenetic placement of the new genus within Heptapteridae was evaluated through a phylogenetic analysis using high-throughput sequencing of UCEs (Faircloth *et al.* 2012). The genome-based matrix of UCEs included 78 specimens, comprising 59 heptapterids, of which 56 were taken from Silva *et al.* (2021), one specimen of *Cetopsorhamdia nasus* Eigenmann & Fisher, 1916, and two samples of the new genus. Vouchers of the samples are listed in Silva *et al.* (2021), except for *C. nasus* and the new genus, which are deposited in the ichthyological section of the Colección Zoológica de la Universidad del Tolima, Ibagué, Colombia (CZUT-IC) and Colección Zoológica de Referencia del Museo de Ciencias Naturales Federico Carlos Lehmann

Valencia del INCIVA (IMCN), Cali, Colombia (Supporting Information, Table S1).

Whole genomic DNA extractions were carried out using a DNeasy Tissue kit (Qiagen), following the manufacturer's protocols and 2 µl of each sample were quantified using fluorometry (Qubit, Life Technologies) to verify an ideal concentration (> 10 ng/µl). Library preparation, sequencing, and raw data processing were performed at Arbor Biosciences (Ann Arbor, MI, USA). For more details about this procedure, see the DNA extraction and sequencing section in the Material and methods section of Roxo *et al.* (2019). To enrich the libraries we also used a probe set developed for ostariophysan fishes to generate sequence data for about 2700 UCE loci (Faircloth *et al.* 2020).

The standard PHYLUCE pipeline was used for processing target-enriched UCE data (Faircloth 2016). Adapter contamination and low-quality bases were trimmed using the Illumiprocessor software pipeline developed by Faircloth (2013; https://github.com/faircloth-lab/illumiprocessor/). After trimming, we assembled Illumina reads and generated consensus contigs for each species using Velvet (Zerbino and Birney 2008) on VelvetOptimiser (https://github.com/tseemann/VelvetOptimiser). We then used the 'match_contigs_to_probes' program implemented in PHYLUCE to align species-specific contigs to the ostariophysan probe-UCE set (Faircloth *et al.* 2020). We created a fasta file containing all data for all taxa. A custom Python program (seqcap_align_2.py) was used to align contigs using the MAFFT algorithm (Katoh *et al.* 2002) and to perform edge trimming. From the trimmed alignment, we generated a matrix keeping UCEs present in at least 70% of the complete alignment matrix, to perform phylogenetic reconstructions. The matrix is available at Figshare (https://doi.org/10.6084/m9.figshare.28641899.v1). Information about data in the matrix is summarized in Silva *et al.* (2021: supplementary table 1).

We analyzed the concatenated dataset using ML in RAxML v.8.019 (Stamatakis 2014), Bayesian inference (BI) in ExaBayes v.1.4 (Aberer *et al.* 2014), and coalescent-based analyses in ASTRAL-III v.5.6.2 (Zhang *et al.* 2018). We performed ML analyses assuming a GTR+G model applied to the total matrix without partitions. The best tree search was performed under the parameter -N = 5 which specifies the number of alternative runs on distinct parsimony starting trees. The concatenated alignment was also used to perform bootstrap replicates using the autoMRE function for the extended majority-rule consensus tree criterion (available in RAxML v.8; Stamatakis 2014) to assess support for individual nodes. Bayesian analysis of the unpartitioned concatenated was performed with two independent runs, each with two chains (one cold and one heated) with 1 000 000 generations using the GTR+G model. Tree space was sampled every 100 generations to yield a total of 10 001 trees. The convergence of the posterior distribution was assessed examining the effective sample size (ESS) > 200 and evaluating posterior trace distribution in Tracer v.1.6 (Rambaut *et al.* 2014). We generated the 50% most credible set of trees from the posterior distribution of possible topologies using the consensus algorithm of ExaBayes (Aberer *et al.* 2014) (burn-in: 25%; thinning: 500). To account for gene-tree incongruence due to incomplete lineage sorting (ILS; Alda *et al.* 2019), a coalescent analysis of species trees was inferred from individual gene trees using a two-step process. First, we used PHYLUCE to resample the 70% complete matrix by loci and generated a best tree using RAxML for each of those matrices. Then, we used ASTRAL-III v.5.6.2 (Zhang *et al.* 2018) to infer species trees from each of the best tree subsets of loci and generated a majority-rule consensus.

RESULTS

Taxonomic account

Magdalenichthys DoNascimiento, Conde-Saldaña, Albornoz-Garzón & Villa-Navarro gen. nov.

ZooBank registration: urn:lsid:zoobank.org:act:3D9186FC-1D47-4E6F-8676-2CF3172216B3.

Type species: Magdalenichthys lundbergi DoNascimiento, Villa-Navarro, Ortega-Lara, Albornoz-Garzón, Méndez-López & Conde-Saldaña sp. nov.

Diagnosis: A member of the tribe Heptapterini as defined by Silva *et al.* (2021). *Magdalenichthys* is distinguished from all other heptapterids by a single autapomorphy: posterolateral corner of lateral ethmoid with pointed posterior process, extending parallel and adjacent to the lateral margin of neurocranium, contacting the lateral margin of frontal, at level of anterior region of orbitosphenoid (vs. posterolateral region of lateral ethmoid devoid of any process, ending at posterior articulation with orbitosphenoid) (Fig. 1). Additionally, *Magdalenichthys* can be recognized from all members of Heptapterini (except *Phenacorhamdia* Dahl, 1961) by having a prognathous mouth (vs. terminal, subterminal, or ventral). *Magdalenichthys* differs from *Phenacorhamdia* by having an upper caudal-fin lobe longer than the lower lobe (vs. lower caudal-fin lobe longer) and hemal spines of vertebrae dorsal to insertion of anal fin simple (vs. bifid). Another character useful for its recognition among Heptapterini species from the Magdalena basin (except *Imparfinis timana* Ortega-Lara, Milani, DoNascimiento, Villa-Navarro & Maldonado-Ocampo, 2011) is the adipose-fin shape roughly rectangular [vs. rounded in *Cetopsorhamdia boquillae* Eigenmann, 1922 or triangular in *Cetopsorhamdia molinae* Miles, 1943, *Cetopsorhamdia nasus*, *Imparfinis nemacheir* (Eigenmann & Fisher, 1916), and *Imparfinis usmai* Ortega-Lara, Milani, DoNascimiento, Villa-Navarro & Maldonado-Ocampo, 2011], being further and easily recognized from *I. timana* by its shorter maxillary barbel, never surpassing the distal edge of the pectoral fin (vs. extending at least to the pelvic-fin base), and pelvic-fin origin at vertical though dorsal-fin origin or slightly posterior (vs. inserted at or slightly posterior to middle of dorsal-fin base).

Included species: Magdalenichthys lundbergi sp. nov., *Magdalenichthys mompox* sp. nov., *Magdalenichthys poira* sp. nov., *Magdalenichthys yariguies* sp. nov.

Etymology: In allusion to the Magdalena River basin, remarking on the restricted geographic distribution of this heptapterid genus to the Cauca and Magdalena rivers, which together form the main hydrographic basin of the trans-Andean region of Colombia, framed by the Western, Central, and Eastern

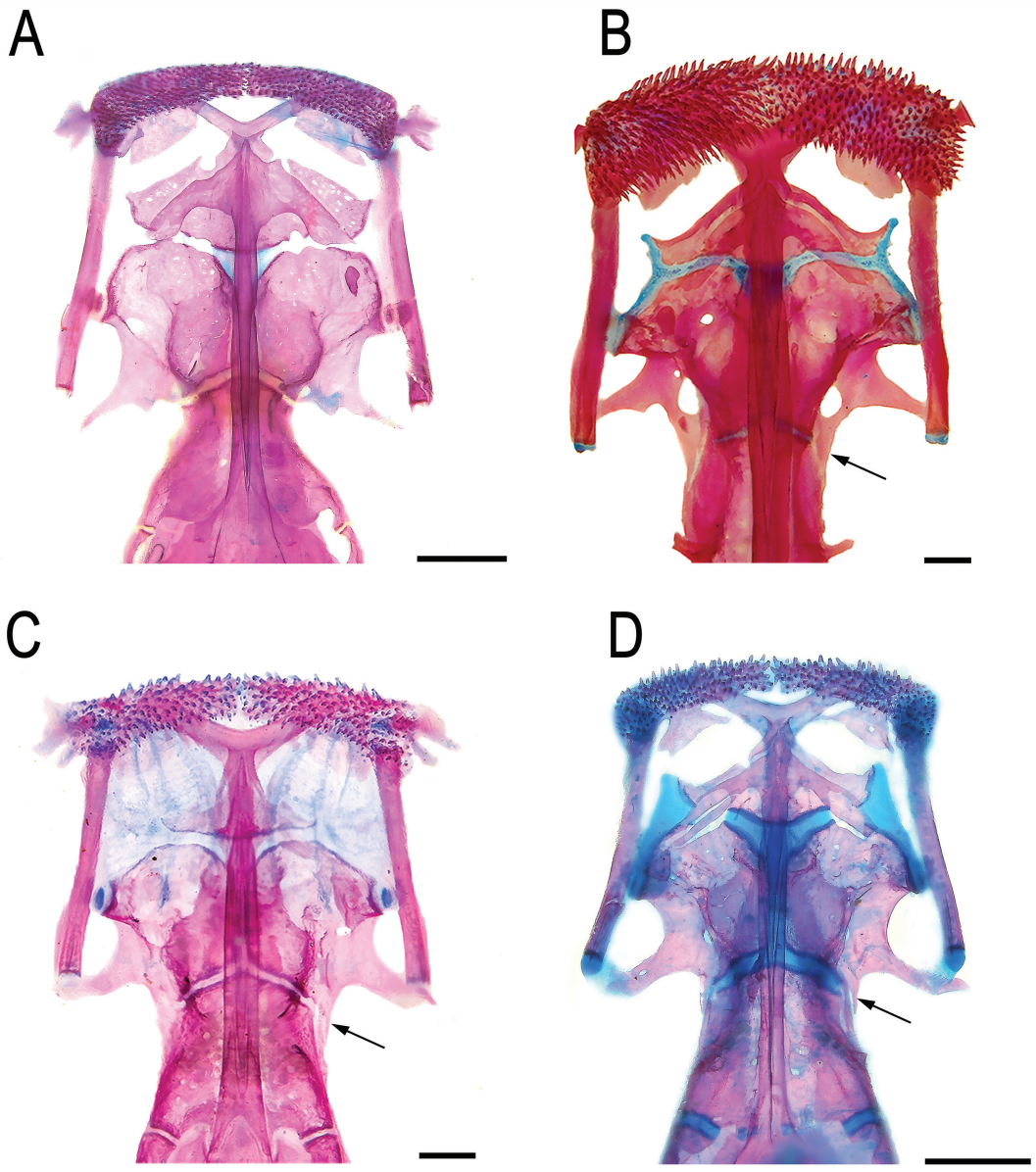

Figure 1. Ventral view of anterior region of cranium of (A) *Phenacorhamdia anisura*, IAvH-P 7932, 41 mm SL; (B) *Magdalenichthys lundbergi*, paratype, IMCN 3506, 87.1 mm SL; (C) *Magdalenichthys poira*, paratype, CZUT-IC 8624, 44.7 mm SL; (D) *Magdalenichthys yariguies*, paratype, IAvH-P 17732, 46.8 mm SL. Arrows indicate diagnostic posterior process of lateral ethmoid of species of *Magdalenichthys* species. Scale bars = 1 mm.

cordilleras, the most salient feature of the Colombian geomorphology. Gender masculine.

Magdalenichthys lundbergi **DoNascimiento, Villa-Navarro, Ortega-Lara, Albornoz-Garzón, Méndez-López & Conde-Saldaña sp. nov.**

(Figs 2–3; Table 1)

ZooBank registration: urn:lsid:zoobank.org:act:E4A72405-C852-4FDF-83EF-F1C2B864AA72.

Holotype: CZUT-IC 25785 (80.9 mm SL); Colombia, Quindío, Armenia, río Verde, tributary of río Quindío, río La Vieja drainage, Cauca River sub-basin, 04°23'43"N 75°45'60"W, 1105 m a.s.l.; J.L. Lozano & G. Murcia, 26 Oct 2017.

Paratypes: CIUA 3841 (1, 62.3 mm SL); Caldas, Neira, río Tareas, tributary of río Tapias, 05°13'22.1"N 75°38'14.2"W, 859 m a.s.l.; J.G. Ospina-Pabón, 8 Mar 2015. CIUA 3843 (2, 46.0–63.5 mm SL); Caldas, Neira, río Tapias, close to the bridge, 05°13'23.8"N 75°38'16.4"W, 853 m a.s.l.; J.G. Ospina Pabón, 3 Mar 2015. CIUA 3856 (1, 69.3 mm SL); Caldas, Río Sucio, río Sucio, tributary of río Supía, 05°22'44.6"N 75°36'57.9"W, 773 m a.s.l.; J.G. Ospina Pabón, 10 Mar 2015. CIUA 3929 (1, 50.5 mm SL); Caldas, Viterbo, vereda La Merced, río Risaralda, 05°05'19.7"N 75°51'15"W, 983 m a.s.l.; J.G. Ospina Pabón, 5 Dec 2014. CIUA 3961 (2, 59.4–75.2 mm SL); Caldas, Belalcázar, quebrada El Zancudo, tributary of río Risaralda, 04°57'51.3"N

Figure 2. Left lateral, dorsal, and ventral views of *Magdalenichthys lundbergi*, CZUT-IC 25785, holotype, 80.9 mm SL; Colombia, Quindío, Armenia, río Verde, tributary of río Quindío, río La Vieja drainage, río Cauca basin. Scale bar = 1 cm.

75°51’30.2”W, 941 m a.s.l.; J.G. Ospina Pabón; 7 Dec 2014. CIUA 3982 (1, 51.5 mm SL); Caldas, Viterbo, río Guarne, tributary of río Risaralda, 05°05’29”N 75°52’04”W, 986 m a.s.l.; J.G. Ospina-Pabón, 6 Dec 2014. CIUA 5399 (1, 27.9 mm SL); Valle del Cauca, Alcalá, quebrada Los Ángeles, 4.71324°–75.8529°; J. Herrera, 10 Feb 2019. CIUA 5400 (1, 73.5 mm SL); Caldas, Belalcázar, quebrada El Zancudo, 4.96425°–75.85837°; D. Valencia, 11 Feb 2019. CIUA 7985 (10, 39.2–72.0 mm SL); Valle del Cauca, Bugalagrande, río Bugalagrande, 04°10’46.9”N 76°08’54.2”W; J. Ospina-Pabón, V.M. Medina Ríos, D. Restrepo Santamaría, 1 Sep 2022. CZUT-IC 12230 (3, 29.1–68.7 mm SL); Quindío, Armenia, río Quindío, tributary of río La Vieja, 04°23’45”N 75°45’47”W; L. Arrieta & I. Pareja, 1 Jun 2014. CZUT-IC 12368 (8, 35.9–81.5 mm SL); Quindío, Calarcá, río Quindío, tributary of río La Vieja, 04°31’47”N 75°38’25”W; A. Ortega-Lara, 1 Sep 2004. CZUT-IC 12397 (6, 24.2–75.3 mm SL); Quindío, Pijao, río Barragán, tributary of río Quindío, río La Vieja drainage, Cauca River sub-basin, 04°20’02”N 75°42’09”W, A. Ortega-Lara, 1 Sep 2004. CZUT-IC 12408 (4, 21.6–59.2 mm SL); Quindío, río Barragán, tributary of río Quindío, río La Vieja drainage, Cauca River sub-basin, 04°20’02”N 75°42’09”W; A. Ortega-Lara, 7 Dec 2004. CZUT-IC 18353 (1, 70.5 mm SL); Valle del Cauca, Yotoco, río Mediacanoa, tributary of Cauca River, 03°54’17”N 76°23’56”W, 993 m a.s.l.; A. Ortega-Lara & G. Sánchez-Garcés, 3 Aug 2017. CZUT-IC 18829 (4, 20.7–44.8 mm SL); Valle del Cauca, Zarzal, río La Paila, tributary of Cauca River, 04°18’36”N 76°02’57”W, 952 m a.s.l.; J.G. Albornoz-Garzón, J.E. García-Melo & B. Melo, 20 Aug 2017. CZUT-IC 19240 (2, 41.1–46.2 mm SL); Quindío, río Verde, tributary of río Quindío, río La Vieja drainage, Cauca River sub-basin, 04°23’43”N 75°45’60”W, 1105 m a.s.l.; J.L. Lozano & G. Murcia, 26 Oct 2017. CZUT-IC 19332 (2, 30.7–61.4 mm SL); Quindío, río Verde, tributary of río Quindío, río La Vieja drainage, Cauca River sub-basin, 04°23’43”N 75°45’60”W, 1105 m a.s.l.; J.L. Lozano & G. Murcia, 26 Dec 2017. CZUT-IC 19392 (1, 58.8 mm SL, 1 c&s, 49.8 mm SL); Quindío, Armenia, río Verde, tributary of río Quindío, río La Vieja drainage, Cauca River sub-basin, 04°23’43”N 75°45’59”W, 1105 m a.s.l.; J.L. Lozano & G. Murcia, 28 Jan 2018. CZUT-IC 19240 (2, 41.1–53.2 mm SL); collected with holotype. CZUT-IC 20459 (4,

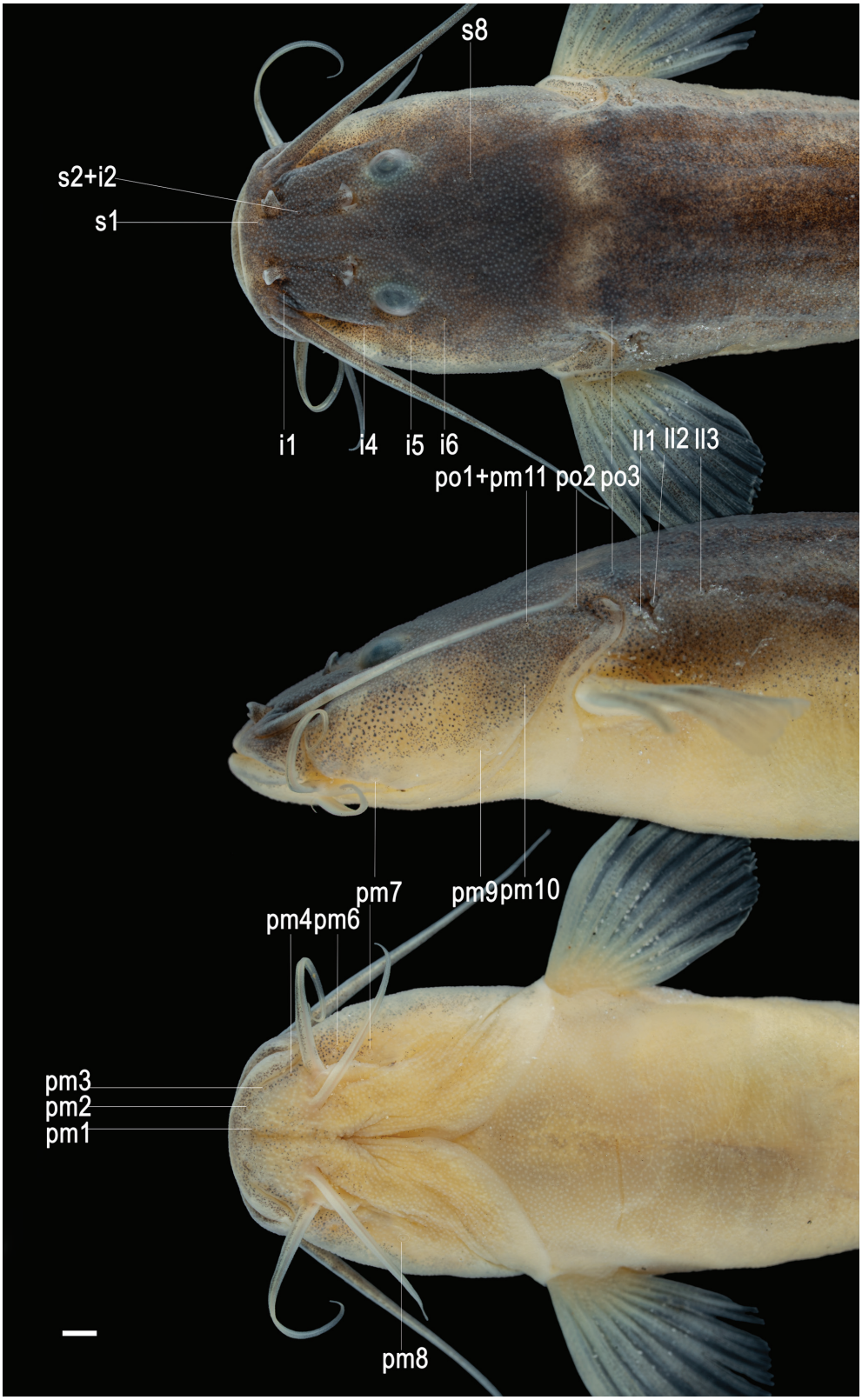

Figure 3. Dorsal, lateral, and ventral views of head, showing cephalic laterosensory pores in *Magdalenichthys lundbergi*, paratype, CIUA 3929, 50.5 mm SL. Abbreviations: i, infraorbital; pm, preoperculo-mandibular; po, postotic; s, supraorbital; ll, lateral line. Scale bar = 1 mm. Photographs by J.L. Londoño-López, used with permission.

Table 1. Morphometric data for holotype and paratypes (17) of *Magdalenichthys lundbergi*, holotype and paratypes (8) of *Magdalenichthys mompox*, holotype and paratypes (22) of *Magdalenichthys poira*, and holotype and paratypes (8) of *Magdalenichthys yariguies*

	M. lundbergi				*M. mompox*				*M. poira*				*M. yariguies*			
	H[a]	R[b]	M[c]	S.D.	H	R	M	S.D.	H	R	M	S.D.	H	R	M	SD
Standard length (mm)	80.9	43.5–80.9	61	11.5	38	30.3–38.0	32.8	2.3	45.2	23.1–55.1	39	7.6	67.9	40.3–67.9	52.4	9.6
Percent of standard length																
Body depth	13.4	9.8–18.3	13.7	1.8	13.7	11.7–16.1	13.7	1.4	11.7	9.2–16.6	12.4	1.8	10.7	9.3–13.0	10.7	1.1
Cleithral width	14.1	13.7–17.4	15.8	0.9	17	15.3–19.1	17.1	1.1	15.6	14.0–18.2	16	1	12.8	12.8–15.2	13.9	0.8
Predorsal length	36.6	35.2–41.5	38.4	1.8	37.5	35.3–40.5	38.5	1.8	37.2	32.2–38.8	36	1.8	33.6	33.6–42.5	38.2	2.9
Dorsal-fin base	12.4	10.1–12.9	11.6	0.7	12.3	11.0–14.5	12.5	1.1	12.5	10.0–15.2	12.9	1.2	11.8	11.4–12.7	12	0.5
Dorsal fin to adipose fin	14.6	12.7–17.8	15.2	1.5	18.9	14.8–19.2	16.9	1.5	14.6	13.9–21.1	17.2	2.1	18.4	14.7–18.5	17.3	1.4
Preadipose length	64.8	62.4–67.8	64.8	1.6	67.7	65.6–71.1	68.2	1.9	64.5	61.6–69.7	66.1	2	66.6	64.0–68.9	66.2	1.8
Adipose-fin length	29.8	22.8–29.8	26.5	1.7	19.4	17.5–20.9	19	1.2	27.1	17.6–30.2	25.6	2.6	28.5	26.2–28.9	27.7	1.1
Prepelvic length	38	35.1–42.6	39	1.9	42.2	42.0–47.9	45.3	2.3	37.9	37.6–43.2	40.2	1.5	35.4	35.4–41.5	39	2
Preanal length	64.8	63.3–68.2	65.3	1.5	65	65.0–70.9	68	1.9	66	60.0–70.8	66.6	2.7	63.9	62.2–66.6	64.6	1.6
Anal-fin base	14.1	11.7–14.4	12.9	0.9	12.7	9.9–13.5	12	1.2	12.6	11.9–16.7	13.4	1.4	18.1	15.6–18.1	16.8	1
Caudal-peduncle length	22.3	20.1–24.2	21.8	1.3	22.4	18.6–22.4	20.1	1.4	21.3	18.1–24.1	22	1.5	19.2	16.3–19.3	17.8	1.2
Caudal-peduncle depth	5.5	5.5–7.5	6.5	0.5	7.5	6.9–7.9	7.5	0.3	5.8	5.3–7.5	6.5	0.6	6.8	6.8–7.5	7.1	0.3
Upper caudal-fin lobe length	20.8	15.2–23.0	20.4	2.1	21.4	20.3–25.4	22.5	1.5	26.3	19.6–29.7	23.5	2.8	25.7	19.6–25.7	22.2	1.9
Lower caudal-fin lobe length	17.4	16.0–20.5	18.4	1.3	22.5	21.9–24.9	23.4	0.9	22.2	15.9–23.0	19.9	1.9	16.3	16.3–19.4	18	1.1
Head length	20	19.3–23.3	20.7	1.1	23.6	22.9–25.1	24.1	0.8	21.9	18.4–22.1	20.2	1.1	16.7	16.7–20.4	19.4	1.2
Percent of head length																
Head width	74.1	63.0–98.2	78.3	7.8	59.5	53.6–78.0	62	8.1	70.9	68.0–88.9	77.6	4.6	65.5	65.5–75.2	69.3	3.6
Head depth	60.9	41.1–62.6	54	5.6	49.3	49.3–69.9	56.3	6.2	46.6	41.8–60.0	51	4.5	51.4	41.0–51.4	44.4	3.5
Mouth gape	43.1	36.1–43.7	39.6	2.4	36.3	28.7–36.3	31.4	2.6	48.4	41.3–53.5	49.3	2.8	41.8	35.4–41.8	39	2.3
Snout length	39.8	36.0–44.4	40.6	1.9	42.8	38.0–42.8	41.1	1.5	34.6	34.2–42.5	38.6	2.3	39.5	37.3–42.6	39.6	2
Fleshy interorbital	26.7	22.7–28.5	26.2	2	26.5	20.9–26.5	23.9	1.7	26.9	20.3–27.7	24.7	2.2	28.9	23.9–28.9	26.4	1.5
Eye diameter	9.3	9.3–12.3	11.3	0.9	11	9.1–12.6	11	1.1	12	11.9–17.8	14.3	1.4	10.6	7.0–11.7	9.1	1.5
Maxillary-barbel length	19	17.5–23.0	20.7	1.5	25.4	22.8–32.1	26.2	2.7	21.6	17.2–25.8	21.9	2	25.8	24.2–30.9	27.6	2.3
Outer mental-barbel length	11.3	10.6–20.8	13.8	2.3	15.9	11.8–17.6	16.1	1.8	14.1	10.3–17.1	14.3	1.8	13.4	13.4–17.7	15.3	1.2
Inner mental-barbel length	8.6	8.6–12.0	10.3	0.8	13.3	12.5–15.8	14.1	1.2	11.1	8.4–12.9	11.1	1.4	9.4	9.4–13.1	11.4	1

[a]H: holotype. [b]R: range. [c]M: arithmetic mean.

46.7–62.3 mm SL), Caldas, Anserma, río Risaralda, 05°10'30"N 75°49'04"W, 1040 m a.s.l.; J.L. Lozano, 12 Dec 2018. IMCN 3506 (20, 39.2–85.2 mm SL, 2 c&s, 78.8–87.7 mm SL); Cauca, Santander de Quilichao, río Quinamayó, tributary of Cauca River sub-basin, 03°06'29.6"N 76°32'13.4"W, 975 m a.s.l.; A. Ortega-Lara, 21 Apr 2004.

Diagnosis: Magdalenichthys lundbergi differs from all its congeners by number of vertebrae (36–37 vs. 32–33 in *M. mompox*, 38–39 in *M. poira*, 40 in *M. yariguies*). *Magdalenichthys lundbergi* is distinguished from *M. poira* and *M. yariguies* by having five or more dentary tooth rows (vs. four). *Magdalenichthys lundbergi* is distinguished from *M. mompox* and *M. yariguies* by having the adipose-fin origin opposite to the anal-fin origin (vs. posterior). *Magdalenichthys lundbergi* further differs from *M. mompox* by having a parabolic contour of the head in dorsal view, with lateral profiles convex (vs. rectangular, with lateral profiles straight); fewer gill rakers on first arch (3–5 vs. 7–8); first dorsal-fin pterygiophore inserted posterior to neural spine of vertebrae 10–11 (vs. vertebra 9); first anal-fin pterygiophore inserted posterior to hemal spine of vertebrae 23–24 (vs. vertebra 21); upper caudal-fin lobe distinctively longer than the lower lobe (vs. both lobes subequal); shorter caudal-fin lower lobe (16–20.5% of SL vs. 21.9–24.9%); fewer caudal-fin branched rays (13 vs. 15); shorter prepelvic length (35.1–42.6% of SL vs. 42–47.9%); longer adipose-fin base (22.8–29.8% of SL vs. 17.5–20.9%); wider mouth (36.1–43.7% of HL vs. 28.7–36.3%); shorter maxillary barbel (17.5–23% of HL vs. 22.8–32.1%); and shorter inner mental barbel (8.6–12% of HL vs. 12.5–15.8%). *Magdalenichthys lundbergi* further differs from *M. poira* by having modally fewer branched rays in the upper lobe of the caudal fin (six vs. seven); translucent or pale nuchal band inconspicuous and narrow in small specimens, faded or absent in large specimens (vs. conspicuous and wide in specimens of all sizes); pale spot at dorsal-fin origin narrow in specimens of up to 72.1 mm SL, absent in larger specimens (vs. wide and triangular, always present in specimens of all sizes); and adipose fin dusky (vs. hyaline). *Magdalenichthys lundbergi* is further distinguished from *M. yariguies* by having fewer anal-fin principal (segmented) rays (9–10 vs. 11–12); insertion of anal fin extending posteriorly to hemal spine of vertebrae 29–30 (vs. vertebrae 33–34), which is externally reflected in a longer caudal peduncle in *M. lundbergi* (20.1–24.2% of SL vs. 16.3–19.3%); shorter anal-fin base (11.7–14.4% of SL vs. 15.6–18.1%); and shorter maxillary barbel (17.5–23% of SL vs. 24.2–30.9%).

Description: Morphometric data in Table 1. Refer to Figure 2 for general appearance. Small heptapterine catfish (largest specimen 80.9 mm SL), with elongated body, elliptical in cross-section at dorsal-fin origin (longest axis vertical), progressively more compressed to caudal region. Dorsal profile slightly convex from snout tip to occipital region, straight immediately posterior to this point to adipose-fin origin, sloping ventrally along adipose-fin base to origin of procurrent caudal-fin rays, and slightly ascending along dorsal membrane supported by procurrent caudal-fin rays. Ventral profile straight to pelvic-fin insertion, slightly concave to anal-fin origin, dorsally sloping along anal-fin base, straight along caudal peduncle to origin of procurrent caudal-fin rays and slightly descending along ventral membrane supported by procurrent caudal-fin rays.

Head depressed, parabolic in dorsal view, dorsally covered by thin skin. Cheek laterally bulged with muscular mass of adductor mandibulae, but muscle not reaching dorsally onto skull roof. Snout short and rounded. Mouth slightly prognathous. Premaxillary teeth arranged in a rhomboidal patch of 5*–9 medial and 8*–11 lateral irregular rows of minute conical teeth. Lower jaw slightly longer than upper jaw. Dentary teeth in 5–8 (7) irregular rows of minute conical teeth, similar to those on premaxilla. Maxillary barbel reaching base of unbranched pectoral-fin ray. Conspicuous groove accommodating anterior part of maxillary barbel along sides of head, extending posteriorly to vertical through posterior margin of posterior nares. Bases of outer and inner mental barbels in a straight line. Mental barbels not reaching base of pectoral fin. Outer mental barbel surpassing branchiostegal membrane. Inner mental barbel reaching edge of branchiostegal membrane. Small subcutaneous eye, dorsal in position and twice longer horizontally than vertical diameter. Anterior naris tubular. Posterior naris closer to anterior margin of eye than to anterior naris, anteriorly bordered by a low fleshy margin. Anterior and posterior internarial widths equal. Nares disposed in a squared arrangement. Branchiostegal membrane free, supported by eight (2)* or nine (1) rays and joined to isthmus only at anteriormost point. Gill rakers on first arch 3–5 (one c&s specimen asymmetrically with one and two gill rakers), located along anterior margin of ceratobranchial.

Lateral line canal complete, reaching caudal skeleton. Supraorbital pore s1 medially adjacent to anterior naris; s2 + i2 pore slightly closer to anterior naris (Fig. 3), at distal end of posteriorly directed membranous tubule, originating from commissure connecting supraorbital and infraorbital canals; s3 pore not visible externally, inside posterior naris, adjacent to its posterior margin, at notch of cutaneous membrane. Contralateral supraorbital canals connected medially by epiphyseal membranous branch, dorsal to posterior portion of anterior fontanel, without superficial pore; s8 pore (parietal branch) arising from a posteriorly directed membranous canal, externally located posterior to eye, at level of medial margin of eye; s4 and s7 branches and pores absent. Infraorbital pore i1 laterally adjacent to anterior naris, between naris and maxillary barbel base; i3 pore posterior to maxillary barbel base; i4 pore slightly anterior to vertical through anterior margin of eye; i5 pore ventral to posterior region of eye; i6 pore posterior to eye, aligned with ventral margin of eye. Pterotic branch (po2) at posterolateral corner of pterotic. Dentary with seven pores of preoperculo-mandibular canal. Submental pores (pm1) paired. Sixth and seventh mandibular pores approximately at same vertical level, and seventh pore just anterior to lateral articulation between dentary and anguloarticular bones. Subpreopercular ossicle with one pore (pm8). Preopercle with two pores, anterior pore (pm9) originating from membranous tubule lateral to interopercle and posterior pore (pm 10) from membranous tubule passing lateral to ventral portion of opercle. Last preopercular pore (po1 + pm11) at end of membranous tubule, dorsal to dorsoposterior portion of opercle. Axillary branch (ll1) ventral, running posterior to supracleithrum.

Precaudal vertebrae 9 (1)–10 (2), thoracic vertebrae 7 (1), 8 (1) or 9 (1), and caudal vertebrae 27, totalling 36–37

vertebrae. Ribs seven (1) or eight (2). Pectoral fin with i,7 (13)*–8 (7) rays. First pectoral-fin ray (unbranched) soft and shorter than first branched ray. Second branched ray longest. Distal margin of pectoral fin convex. Pelvic fin with i,5 rays. First pelvic-fin ray (unbranched) thick and shortest, second and third branched rays longest. Pelvic-fin origin opposite to dorsal-fin origin, at vertical through vertebra 13 (2). Dorsal fin lacking spinelet, with one unbranched and five (1), six* (29) or seven (3) branched rays (one specimen out of 18 from with five branched rays), supported by seven pterygiophores. Dorsal-fin margin convex, its unbranched ray slightly shorter than first branched ray; first three branched rays subequal. First dorsal-fin pterygiophore inserted posterior to neural spine of vertebrae 10 (1) or 11 (2) and last pterygiophore anterior to neural spine of vertebrae 16 (1) or 17 (2). Adipose fin long, almost rectangular with attenuated ends and posterior lobe free. Adipose-fin origin at vertical through anal-fin origin. Anal fin with 2 (1)–3 (2) procurrent (unsegmented) rays, 2 (8)–3 (10)* unbranched rays, and six* (8), seven (8), or eight (2) branched rays for a total of nine (16) or 10 (4) principal rays. Posteriormost ray (branched) individually associated to last pterygiophore. Anal-fin distal margin rounded. Anal fin supported by 10 (1)–11 (2) pterygiophores. First anal-fin pterygiophore posterior to hemal spine of vertebrae 23 (2)–24 (1) and last pterygiophore anterior to hemal spine of vertebrae 29 (1)–30 (2). Caudal fin deeply forked with i,7 + 7,i principal rays (two c&s specimens of 35.9 and 68.7 mm SL with either six branched rays in lower or in upper lobe, respectively). Upper lobe of caudal fin distinctly longer than lower lobe, upper lobe generally pointed and lower lobe generally rounded. Procurrent caudal-fin rays 13 (2) or 15 (1) dorsal and 13 (1), 14 (1) or 16 (1) ventral, located posterior to vertebra PU_6. Posteriormost two dorsal and two (1) or three (2) ventral procurrent caudal-fin rays segmented. Caudal skeleton PH + 1 + 2,3 + 4 + 5. Long epural present.

Pigmentation in alcohol: Overall ground coloration dark brown. Dorsal surface of head dark. Pale or translucent (superficial muscles of dorsum visible through it) band inconspicuous and narrow, between dorsal corners of branchial openings in small specimens, fading or disappearing in specimens larger than 70 mm SL. Dorsal surface posterior to nuchal band dark. Transverse elliptical or ovoid pale spot at dorsal-fin origin in specimens of 72.1 mm SL or smaller; spot absent in larger specimens. Base of dorsal and adipose fins with darker region along sides. Ventral surface of head and body pale, with sparse chromatophores posterior to ventral fins. Cheeks slightly lighter than remaining dorsal surface of head, with translucent horizontal band (cheek muscles visible through it) in small specimens. Dark chromatophores aligned along lateral line and myosepta. Maxillary barbel darkly pigmented, darker dorsally. Lateral surface of mental barbels with dark chromatophores, denser on outer barbel. Fin rays and adipose fin dusky, with numerous chromatophores. Interradial membrane of rayed fins hyaline.

Distribution: Magdalenichthys lundbergi is found in the main tributaries of the upper basin of the Cauca River (Quinamayó, Mediacanoa, La Vieja, and Risaralda rivers) (Fig. 4).

Habitat and ecological notes: Magdalenichthys lundbergi is found in sloped sectors of small to middle width (3–25 m) rivers, with turbulent flow and gravel bottom with rocks and boulders, along an elevational gradient from 895 to 1669 m a.s.l. The species can be found syntopically with *Characidium chancoense* Agudelo-Zamora, Ortega-Lara & Taphorn, 2020, *Saccodon dariensis* (Meek & Hildebrand, 1913), *Astyanax* sp., *Creagrutus brevipinnis* Eigenmann, 1913, *Hemibrycon caucanus* (Eigenmann, 1913), *Hemibrycon dentatus* (Eigenmann, 1913), *Brycon henni* Eigenmann, 1913, *Chaetostoma leucomelas* Eigenmann, 1918, and *Cetopsorhamdia nasus*. Stomachs of two dissected specimens contained remains of larvae of aquatic insects including: Trichoptera (Leptoceridae and Hidroptilidae), Plecoptera (Perlidae), and Diptera (Chironomidae), and of terrestrial groups such as Hymenoptera (Formicidae) and Orthoptera. Gonads of three dissected specimens corresponded to two ovate females with 299 (59.6 mm SL) and 358 ovocites (54.4 mm SL), and a mature male (36 mm SL). The species was informally categorized as Vulnerable in Ortega-Lara *et al.* (2022).

Etymology: The species name is dedicated to John G. Lundberg, in recognition of its seminal contributions to the systematics of pimelodoid and heptapterid catfishes, and for being an inspiring milestone in the first author's career.

Magdalenichthys mompox **DoNascimiento, Villa-Navarro, Albornoz-Garzón, Méndez-López & Conde-Saldaña sp. nov.**

(Figs 5–6; Table 1)

ZooBank registration: urn:lsid:zoobank.org:act:D309881B-DE1C-45F6-BAB8-2C6D334BA90A.

Holotype: CZUT-IC 25911 (38.0 mm SL); Colombia, Antioquia, Cáceres, Cauca River; 07°41'12"N 75°16'30"W, 100 m a.s.l.; D. Montoya-Ospina & D. Bedoya, 8 Feb 2019.

Paratypes: Colombia: CIUA 8149 (1, 37.7 mm SL); Tolima, Ortega, río Tetuan, 03°51'10.3"N 75°16'24.2"W; J.G. Ospina Pabón, D. Restrepo Santamaría, J.L. Londoño López, 6 Mar 2023. CZUT-IC 15098 (10, 24.7–34.2 mm SL, 1 c&s, 30.9 mm SL); Cesar, El Copey, río Ariguaní, tributary of río Cesar; 10°16'05"N 73°59'14"W, 163 m a.s.l.; J.G. Albornoz-Garzón & G. Beltrán, 22 Oct 2015. CZUT-IC 20495 (1, 33.2 mm SL, 1 c&s, 33.4 mm SL); collected with holotype. IAvH-P 21928 (3, 21.1–31.5 mm SL); Colombia, Antioquia, Cáceres, Cauca River at Puerto Bélgica, 07°41'25.6"N 75°16'22.34"W; D. Montoya-Ospina, 4 Feb 2019.

Diagnosis: Magdalenichthys mompox differs from all its congeners by having a rectangular contour of the head in dorsal view, with lateral profiles straight (vs. parabolic, with lateral profiles convex); more numerous gill rakers on first arch (7–8 vs. 3–5 in *M. lundbergi*, 5–6 in *M. poira*, 3–4 in *M. yariguies*); fewer vertebrae (32–33 vs. 36–37 in *M. lundbergi*, 38–39 in *M. poira*, 40 in *M. yariguies*); first dorsal-fin pterygiophore inserted posterior to neural spine of vertebra 9 (vs. vertebrae 10–12); first anal-fin pterygiophore inserted posterior to hemal spine of vertebra 21 (vs. vertebrae 23–25); caudal-fin lobes subequal (vs.

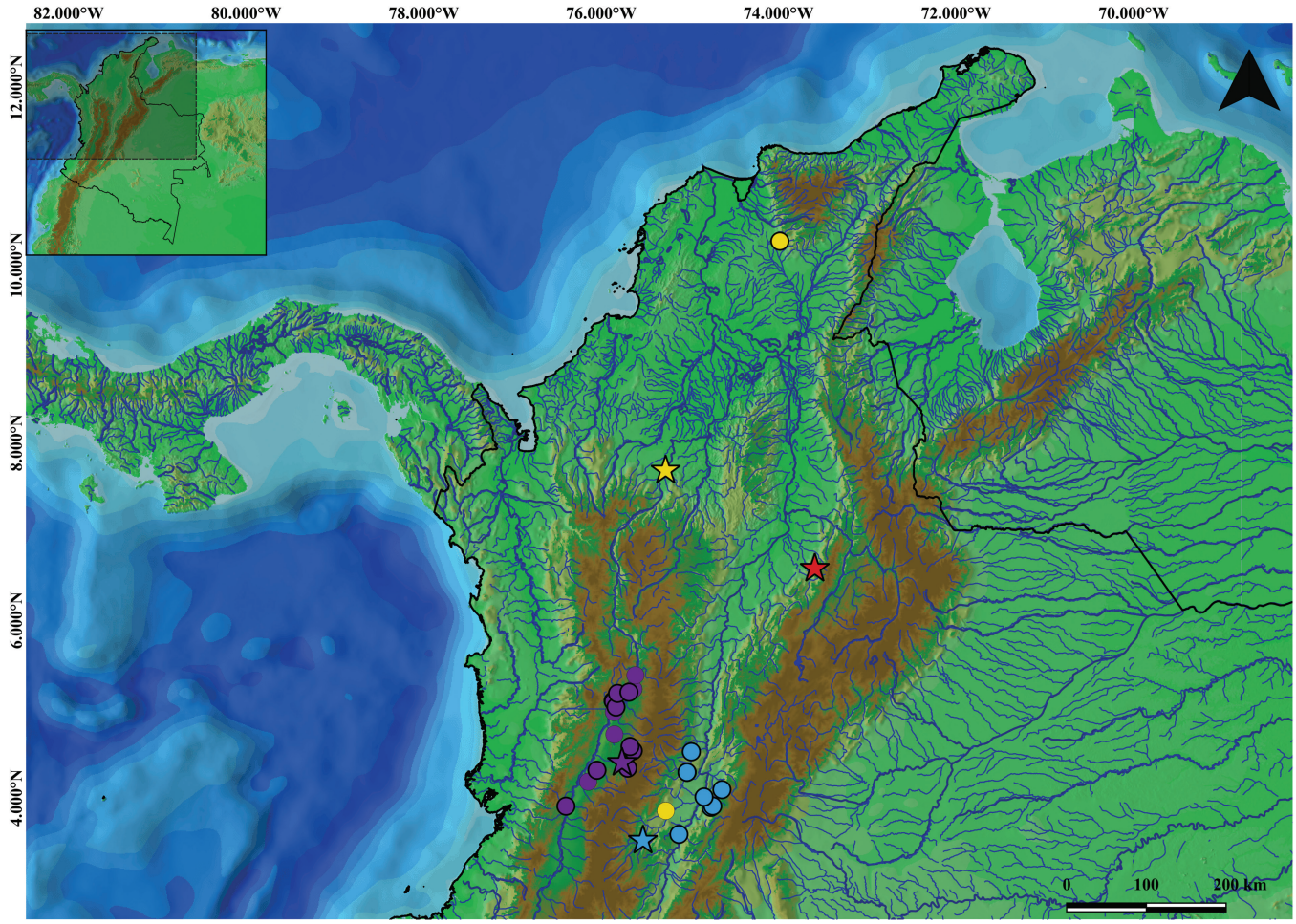

Figure 4. Map of northwestern portion of South America showing the distribution of species of *Magdalenichthys* based in specimens from museum records. Purple: *M. lundbergi*, yellow: *M. mompox*, blue: *M. poira*, red: *M. yariguies*. Stars: type localities. Circles: collection records.

upper-caudal fin lobe distinctively longer than lower lobe); and more numerous caudal-fin branched rays (15 vs. 14 or fewer). *Magdalenichthys mompox* can be additionally distinguished from *M. lundbergi* and *M. poira* by having the adipose-fin origin posterior to the anal-fin origin (vs. origin of both fins at same vertical); narrower mouth (28.7–36.3% of HL vs. 36.1–43.7% in *M. lundbergi*, 41.3–53.5% in *M. poira*); longer maxillary barbel (22.8–32.1% of HL vs. 17.5–23% in *M. lundbergi*, 17.5–23% in *M. poira*); and longer inner mental barbel (12.5–15.8% of HL vs. 8.6–12% in *M. lundbergi*, 8.4–12.9% in *M. poira*). *Magdalenichthys mompox* can be recognized from *M. lundbergi* and *M. yariguies* by having a longer prepelvic length (42–47.9% of SL vs. 35.1–42.6% in *M. lundbergi*, 35.4–41.5% in *M. yariguies*); shorter adipose-fin base (17.5–20.9% of SL vs. 22.9–29.8% in *M. lundbergi*, 26.2–28.9% in *M. yariguies*); and longer caudal-fin lower lobe (21.9–24.9% of SL vs. 16–20.5% in *M. lundbergi*, 16.3–19.4% in *M. yariguies*). *Magdalenichthys mompox* can be recognized from *M. poira* and *M. yariguies* by having a longer head (22.9–25.1% of SL vs. 18.4–22.1% in *M. poira*, 16.7–20.4% in *M. yariguies*). *Magdalenichthys mompox* further differs from *M. poira* by having more ribs (eight vs. six to seven) and fewer number of ventral procurrent caudal-fin rays (12–14 vs. 15–16). *Magdalenichthys mompox* further differs from *M. yariguies* by having fewer principal anal-fin rays (9–10 vs. 11–12); greater cleithral width (15.3–19.1% of SL vs. 12.8–15.2%); and shorter anal-fin base (9.9–13.5% of SL vs. 15.6–18.1%).

Description: Morphometric data in Table 1. Refer to Figure 5 for general appearance. Small heptapterine catfish (largest specimen 38 mm SL), with elongated body, elliptical in cross-section at dorsal-fin origin (longest axis vertical), progressively more compressed to caudal region. Dorsal profile straight from snout tip to occipital region, straight and slightly ascending immediately posterior to this point to dorsal-fin origin, straight along dorsal-fin base to adipose-fin origin, sloping ventrally along adipose-fin base and slightly ascending along dorsal membrane supported by procurrent caudal-fin rays. Ventral profile of head slightly convex, then straight to anal-fin origin, dorsally sloping along anal-fin base to origin of procurrent caudal-fin rays and slightly descending along membrane supported by procurrent caudal-fin rays.

Head depressed, roughly rectangular in dorsal view, dorsally covered by thin skin. Cheek filled with muscular mass of adductor mandibulae, but muscle not reaching dorsally onto skull roof. Snout short and rounded. Mouth slightly prognathous. Premaxillary teeth arranged in a rhomboidal patch of 4–5* medial and 8*–9 lateral irregular rows of minute conical teeth. Lower jaw slightly longer than upper jaw. Dentary teeth

Figure 5. Left lateral, dorsal, and ventral views of *Magdalenichthys mompox*, CZUT-IC 25911, holotype, 38.0 mm SL; Antioquia, Cáceres, Cauca River. Scale bar = 1 cm.

in 4*–5 irregular rows of minute conical teeth, similar to those on premaxilla. Maxillary barbel reaching base of innermost pectoral-fin ray. Conspicuous groove accommodating anterior part of maxillary barbel along sides of head and delimiting dorsal and lateral regions of head. Bases of outer and inner mental barbels in a straight line. Outer mental barbel reaching pectoral-fin origin. Inner mental barbel reaching branchial opening. Small subcutaneous eye, dorsal in position and almost circular. Anterior naris tubular. Posterior naris closer to anterior margin of eye than to anterior naris, anteriorly bordered by a low fleshy margin. Anterior and posterior internarial widths equal. Nares disposed in a squared arrangement. Branchiostegal membrane free, supported by 7 or 8 rays and joined to isthmus only at anteriormost point. Gill rakers of first arch 7–8, located along anterior margin of ceratobranchial.

Lateral line canal complete, reaching caudal skeleton. Supraorbital pore s1 medially adjacent to anterior naris; s2 + i2 pore slightly closer to anterior naris (Fig. 6), at distal end of posteriorly directed membranous tubule, originating from commissure connecting supraorbital and infraorbital canals, closer to supraorbital canal; s3 pore not visible externally, inside posterior naris, adjacent to its posterior margin, at notch of cutaneous membrane. Contralateral supraorbital canals connected medially by epiphyseal membranous branch, dorsal to middle of anterior fontanel, without superficial pore; s8 pore (parietal branch) arising from a posteriorly directed membranous canal, externally located posterior to eye, at level of medial margin of eye; s4 and s7 branches and pores absent. Infraorbital pore i1 laterally adjacent to anterior naris, between naris and maxillary barbel base; i3 pore posterior to maxillary barbel base; i4 pore approximately at vertical through posterior margin of posterior naris; i5 pore at vertical through posterior margin of eye; i6 pore posterior to eye, aligned with ventral margin of eye. Pterotic branch (po2) at posterolateral corner of pterotic. Dentary with seven pores of preoperculo-mandibular canal. Submental pores (pm1) paired. Sixth and seventh mandibular pores approximately at same vertical level. Subpreopercular ossicle with one pore (pm8). Preopercle with two pores, anterior pore (pm9) originating from membranous tubule lateral to interopercle and posterior pore (pm10) from membranous tubule passing lateral to ventral portion of opercle. Last preopercular pore (po1 + pm11) at end of membranous tubule, dorsal to dorsoposterior portion of opercle. Axillary branch (ll1) ventral, running posterior to supracleithrum.

Precaudal vertebrae 9 (1)–10 (1), thoracic vertebrae 7(1) or 8 (1), and caudal vertebrae 23, totalling 32–33 vertebrae. Ribs eight (last rib shortest). Pectoral fin with i,7* (8)–8 (1) rays. First pectoral-fin ray (unbranched) soft and shorter than

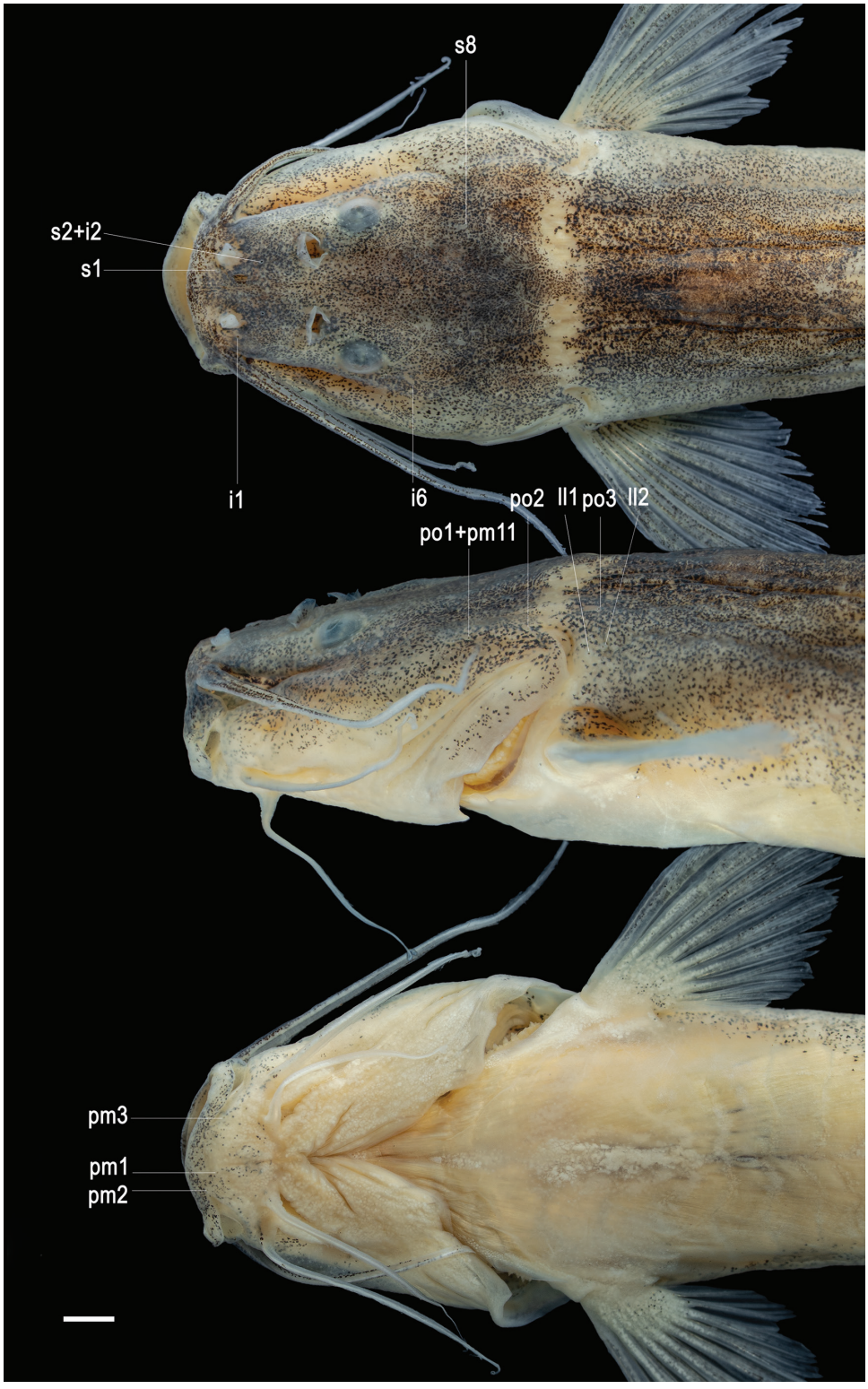

Figure 6 . Dorsal, lateral, and ventral views of head, showing cephalic laterosensory pores in *Magdalenichthys mompox*, paratype, CIUA 8149, 37.7 mm SL. Abbreviations: i, infraorbital; pm, preoperculo-mandibular; po, postotic; s, supraorbital; ll, lateral line. Scale bar = 1 mm. Photographs by J.L. Londoño-López, used with permission.

first branched ray. First branched ray longest. Distal margin of pectoral fin convex. Pelvic fin with i,5 rays. First pelvic-fin ray (unbranched) thick and shortest, second and third branched rays longest. Pelvic-fin origin at level of first branched ray of dorsal fin, at vertical through vertebrae 13 or 14. Dorsal fin lacking spinelet, with one unbranched and six branched rays (one c&s specimen with five branched rays), supported by seven pterygiophores. Dorsal-fin margin convex, its unbranched ray

as long as first branched ray; first three branched rays subequal. First dorsal-fin pterygiophore inserted posterior to neural spine of vertebra 9 and last pterygiophore anterior to neural spine of vertebra 15. Adipose fin long, almost rectangular with attenuated ends and posterior lobe free. Adipose-fin origin at vertical through second unbranched ray of anal fin. Anal fin with 2 (1)–3 (1) procurrent (unsegmented) rays, and 2 (4)–3* (5) unbranched and six* (3) or seven (5) branched rays for a total of nine (5) or ten (3) principal rays. Posteriormost one or two rays (branched) associated with last pterygiophore. Anal-fin distal margin rounded. Anal fin supported by nine pterygiophores. First anal-fin pterygiophore posterior to hemal spine of vertebra 21 and last pterygiophore anterior to hemal spine of vertebra 27. Caudal fin deeply forked with i,7 + 8,i principal rays. Caudal-fin lobes subequal, with lower lobe slightly longer than upper lobe, both lobes pointed. Procurrent caudal-fin rays 13 (1) or 14 (1) dorsal and 12 (1) or 14 (1) ventral, located posterior to vertebra PU_5 (dorsal rays) and to PU_5 or PU_6 (ventral rays). Posteriormost two procurrent caudal-fin rays segmented. Caudal skeleton PH + 1 + 2,3 + 4 + 5. Long epural present.

Pigmentation in alcohol: Overall ground coloration light brown. Minute and numerous melanophores clustered at humeral region. Dorsal surface of head and predorsal area darker than remaining of body surface. Dark streak extending dorsally on surface of snout, between base of maxillary barbel and anterior margin of eye. Conspicuous and narrow pale band posterior to head, between dorsal corners of branchial openings. Cheeks and maxilar groove lighter than remaining surface of head, peppered with sparse chromatophores. Basal portion of maxillary barbel darkly pigmented on dorsal surface. Pale transversely oval spot at dorsal-fin origin. Base of dorsal fin and adipose fin with a dark band along sides. Ventral surface of head and body pale. Adipose fin with sparse chromatophores. Rays of fins with chromatophores. Interradial membrane of fins hyaline.

Distribution: This species has a patchy distribution in three disjunct areas of the Magdalena basin, the lower course of the main channel of the Cauca River, the río Ariguaní, a tributary of the lower basin of the río Cesar, and in the río Tetuan, a tributary of the río Saldaña that drains directly in the upper basin of the Magdalena River (Fig. 4). It is expected that this distribution pattern simply reflects an artifact of sampling.

Etymology: The species name refers to the Cacique Mompoj of the Malibú tribe that once inhabited the region today corresponding to the municipality of Santa Cruz de Mompox, within the so-called Momposina Depression. This indigenous group was exterminated by the Spanish armies of Gerónimo Lebrón and Alonso Martín, during the Cesar massacre of 1540. Used as a noun in apposition.

Magdalenichthys poira **Villa-Navarro, DoNascimiento, Albornoz-Garzón, Méndez-López & Conde-Saldaña sp. nov.**

(Figs 7–8; Table 1)

ZooBank registration: urn:lsid:zoobank.org:act:8FDB875F-DB8E-42AD-A6FF-757D086E0121.

Holotype: CZUT-IC 25786 (45.2 mm SL), Colombia, Tolima, Chaparral, río Guanábanos, tributary of río Saldaña, 03°31'08"N 75°31'50"W; L.J. García-Melo, Y. Lozano & E.O. López-Delgado, 7 Mar 2009.

Paratypes: Tolima: CZUT-IC 807 (17, 22.2–56 mm SL, 1 c&s, 45.2 mm SL); Coello, quebrada Gualanday, tributary of río Coello, 04°18'17"N 75°00'51"W; F.A. Villa-Navarro, A. Ortega-Lara, L.J. García-Melo, N.G. Briñez-Vásquez & P.T. Zúñiga-Upegui, 9 May 2003. CZUT-IC 1619 (5, 38.7–53.8 mm SL); Cunday, río Cunday, tributary of río Prado, 03°54'22"N 74°44'40"W; F.A. Villa-Navarro, L.J. García-Melo, D. Castro Roa & M.E. Herrada-Yara, 18 Aug 2004. CZUT-IC 1621 (4, 40.7–49.2 mm SL); Cunday, río Cunday, tributary of río Prado, 04°01'58"N 74°34'57"W; F.A. Villa-Navarro, L.J. García-Melo, D. Castro Roa & M.E. Herrada-Yara, 23 Aug 2004. CZUT-IC 1624 (8, 24.1–55.9 mm SL); same locality as CZUT-IC 1619; F.A. Villa-Navarro, L.J. García-Melo, D. Castro Roa & M.E. Herrada-Yara, 15 Nov 2004. CZUT-IC 3176 (9, 24.2–62.9 mm SL); collected with holotype. CZUT-IC 5679 (17, 28.3–46.2 mm SL, 1 c&s, 44.8 mm SL); Natagaima, río Anchique, 03°35'19.2"N 75°07'35.7"W, 361 m a.s.l.; M.C. Moreno-Palacios, C. Yara-Ortiz, F.A. Villa-Navarro & E. López, 21 Nov 2010. CZUT-IC 8624 (13, 30.8–55.1 mm SL, 2 c&s, 44.6–45.5 mm SL); same locality as CZUT-IC 807; F.A. Villa-Navarro, 23 Oct 2012. CZUT-IC 11547 (8, 35.9–45.7 mm SL); Natagaima, río Anchique, 03°35'10"N 75°07'54"W; J.G. Albornoz-Garzón, D. Montoya, F.A. Villa Navarro, 7 Feb 2014. IAvH-P 4603 (3, 43.4–47.9 mm SL); Coello, quebrada Gualanday, tributary of río Coello, 04°18'17.5"N 75°02'0.01"W; F.A. Villa-Navarro, L.J. García-Melo, J.A. Maldonado-Ocampo, P.A. Buckup, 21 Apr 2005. IAvH-P 13684 (1, 34.5 mm SL); San Sebastián de Mariquita, río Cuamo, tributary of río Sabandija, 05°08'34.5"N 74°53'58.9"W, 438 m a.s.l.; L.M. Mesa-Salazar & P. Sánchez-Duarte, 17 Oct 2015.

Diagnosis: Magdalenichthys poira is distinguished from all its congeners by the number of vertebrae (38–39 vs. 36–37 in *M. lundbergi*, 32–33 in *M. mompox*, 40 in *M. yariguies*). *Magdalenichthys poira* can be separated from *M. lundbergi* and *M. yariguies* by having modally more branched rays in the upper lobe of the caudal fin (seven vs. six). *Magdalenichthys poira* differs from *M. mompox* and *M. yariguies* by the number of gill rakers on first arch (5–6 vs. 7–8 in *M. mompox*, 3–4 in *M. yariguies*); first dorsal-fin pterygiophore inserted posterior to neural spine of vertebrae 10–11 (vs. vertebra 9 in *M. mompox*, vertebra 12 in *M. yariguies*); and adipose-fin origin at vertical through anal-fin origin (vs. posterior). *Magdalenichthys poira* further differs from *M. lundbergi* by having fewer rows of dentary teeth (four vs. five or more); translucent or pale nuchal band conspicuous and wide in specimens of all sizes (vs. inconspicuous and narrow in small specimens, faded or absent in large specimens); wide triangular spot at dorsal-fin origin always present in specimens of all sizes (vs. narrow transverse spot only present in specimens of 72.1 mm SL or smaller); and adipose fin hyaline (vs. dusky). *Magdalenichthys poira* further differs from *M. mompox* by having a parabolic contour of the head in dorsal view, with lateral profiles convex (vs. rectangular, with lateral profiles straight); fewer ribs (six to seven vs. eight); first anal-fin pterygiophore inserted

Figure 7. Left lateral, dorsal, and ventral views of *Magdalenichthys poira*, CZUT-IC 25786, holotype, 45.2 mm SL; Colombia, Tolima, Chaparral, río Guanábano, río Saldaña drainage, Magdalena River. Scale bar = 1 cm.

posterior to hemal spine of vertebrae 23–25 (vs. vertebra 21); upper-caudal fin lobe distinctively longer than lower lobe (vs. both lobes subequal); fewer caudal-fin branched rays (13–14 vs. 15); more ventral procurrent caudal-fin rays (15–16 vs. 12–14); shorter head (18.4–22.1% of SL vs. 22.9–25.1%); wider mouth (41.3–53.5% of HL vs. 28.7–36.3%); shorter maxillary barbel (17.5–23% of HL vs. 22.8–32.1%); and shorter inner mental barbel (8.4–12.9% of HL vs. 12.5–15.8%). *Magdalenichthys poira* differs from *M. yariguies* by having fewer branched pectoral-fin rays (seven vs. eight); fewer principal (segmented) anal-fin rays (9–10 vs. 11–12); fewer anal-fin pterygiophores (9–10 vs. 11); last anal-fin pterygiophore anterior to hemal spine of vertebra 30 (vs. vertebrae 33–34); more dorsal procurrent caudal-fin rays (14–16 vs. 13); more ventral procurrent caudal-fin rays (15–16 vs. 13–14); wider mouth (41.3–53.5% of HL vs. 35.4–41.8%); and larger eye (11.9–17.8% of HL vs. 7.0–11.7%).

Description: Morphometric data in Table 1. Refer to Figure 7 for general appearance. Small heptapterine catfish (largest specimen 71.4 mm SL), with elongated body, elliptical in cross-section at dorsal-fin origin, progressively more compressed to caudal region. Dorsal profile straight from snout tip to occipital region, slightly convex immediately posterior from this point to dorsal-fin origin, then straight to adipose-fin origin, gently sloping ventrally to posterior end of adipose-fin base, and slightly ascending along caudal peduncle. Ventral profile of head slightly convex, straight along abdomen to anal-fin origin, ascending along anal-fin base and slightly descending along caudal peduncle.

Head depressed, parabolic in dorsal view, dorsally covered by thin skin. Cheek filled with muscular mass of adductor mandibulae, but muscle not reaching dorsally onto skull roof. Snout short and rounded. Mouth slightly prognathous. Premaxillary teeth arranged in a rhomboidal patch of 4 (2)–5 (1)* medial and eight lateral irregular rows of minute conical teeth. Lower jaw slightly longer than upper jaw. Dentary teeth in four irregular rows of minute conical teeth, similar to those on premaxilla. Maxillary barbel reaching pectoral-fin axil. Conspicuous groove accommodating anterior part of maxillary barbel along sides of head, delimiting dorsal and lateral regions of head. Bases of outer and inner mental barbels in a straight line. Mental barbels not reaching base of pectoral fin. Outer mental barbel reaching branchiostegal membrane. Small subcutaneous eye, dorsal in position and slightly longer horizontally. Anterior naris tubular. Posterior naris closer to anterior margin of eye than to anterior naris, anteriorly bordered by a low fleshy margin. Anterior and posterior internarial widths equal. Nares disposed in a squared arrangement. Branchiostegal membrane free, supported by eight rays and joined to isthmus only at anteriormost point. Gill rakers of first arch 5–6, located along anterior margin of ceratobranchial.

Lateral line canal complete, reaching caudal skeleton. Supraorbital pore s1 medially adjacent to anterior naris; s2 + i2

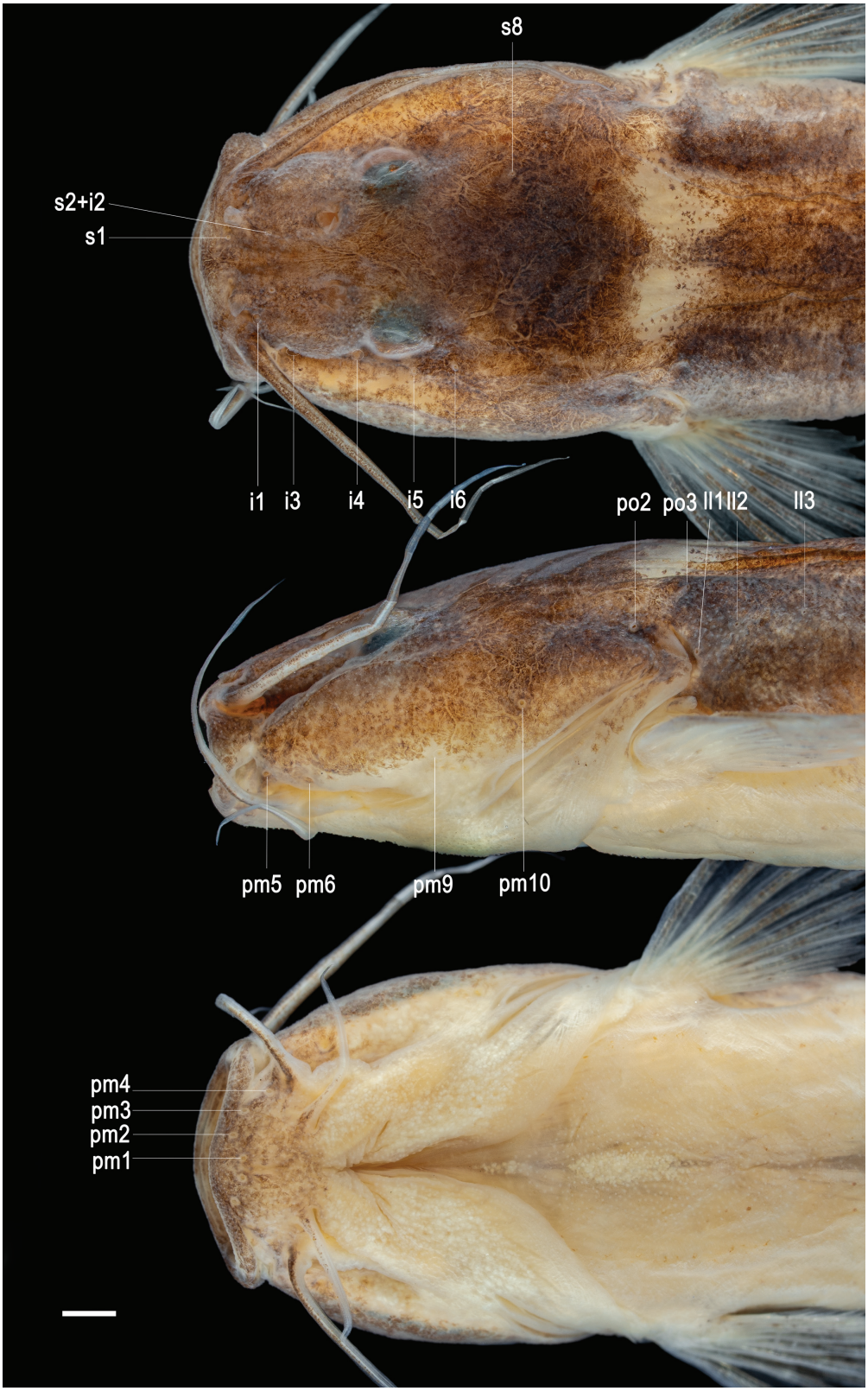

Figure 8 . Dorsal, lateral, and ventral views of head, showing cephalic laterosensory pores in *Magdalenichthys poira*, paratype, CZUT-IC 1621, 49.5 mm SL. Abbreviations: i, infraorbital; pm, preoperculo-mandibular; po, postotic; s, supraorbital; ll, lateral line. Scale bar = 1 mm. Photographs by J.L. Londoño-López, used with permission.

pore slightly closer to anterior naris (Fig. 8), at distal end of posteriorly directed membranous tubule, originating from commissure connecting supraorbital and infraorbital canals, closer to infraorbital canal; s3 pore not visible externally, inside posterior naris, adjacent to its posterior margin, at notch of cutaneous membrane. Contralateral supraorbital canals connected medially by epiphyseal membranous branch, dorsal to anterior fontanel, without superficial pore; s8 pore (parietal branch) arising from a posteriorly directed membranous canal, externally located posterior to eye, at level of medial margin of eye; s4 and s7 branches and pores absent. Infraorbital pore i1 laterally adjacent to anterior naris, between naris and maxillary barbel base; i3 pore posterior to maxillary barbel base; i4 pore at vertical through anterior margin of eye; i5 pore ventral to posterior region of eye; i6 pore at vertical through posterior margin of eye. Pterotic branch (po2) at posterolateral corner of pterotic. Dentary with seven pores of preoperculo-mandibular canal. Submental pores (pm1) paired. Sixth and seventh mandibular pores approximately at same vertical level, and seventh pore just anterior to lateral articulation between dentary and anguloarticular bones. Subpreopercular ossicle with one pore (pm8). Preopercle with two pores, anterior pore (pm9) originating from membranous tubule lateral to interopercle and posterior pore (pm10) from membranous tubule passing lateral to ventral portion of opercle. Last preopercular pore (po1 + pm11) at end of membranous tubule, dorsal to dorsoposterior portion of opercle. Axillary branch (ll1) ventral, running posterior to supracleithrum.

Precaudal vertebrae 10(1)–11 (2), thoracic vertebrae 8 (1) or 9 (2), and caudal vertebrae 28, totalling 38–39 vertebrae. Ribs six or seven. Pectoral fin with i,6 (2), 7* (34), or 8 (23) rays. First pectoral-fin ray (unbranched) soft and shorter than first branched ray. First branched ray longest. Distal margin of pectoral fin convex. Pelvic fin with i,5 rays. First pelvic-fin ray (unbranched) thick and shortest, second and third branched rays longest. Pelvic-fin origin opposite to dorsal-fin origin, at vertical through vertebra 14 (2). Dorsal fin lacking spinelet, with one unbranched and six branched rays, supported by seven pterygiophores. Dorsal-fin margin convex, its unbranched ray slightly shorter than first branched ray; first three branched rays subequal. First dorsal-fin pterygiophore inserted posterior to neural spine of vertebrae 10 (1) or 11 (2) and last pterygiophore anterior to neural spine of vertebra 16. Adipose fin long, almost rectangular with attenuated ends and posterior lobe free. Adipose-fin origin at vertical through anal-fin origin. Anal fin with two procurrent (unsegmented) rays, and two* (24), three (1), or four (1) unbranched and six (2), seven (19), or eight (5)* branched rays, for a total of nine (20) or ten* (5) principal rays. Posteriormost ray (branched) individually associated to last pterygiophore. Anal fin supported by 9 (2)–10 (1) pterygiophores. First anal-fin pterygiophore posterior to hemal spine of vertebrae 23 (1) or 25 (2) and last pterygiophore anterior to hemal spine of vertebra 30. Caudal fin deeply forked with i,7 + 7,i principal rays (one single specimen out of 23 with six branched rays in upper lobe). Upper lobe of caudal fin distinctly longer than lower lobe, both lobes generally rounded. Procurrent caudal-fin rays 14 (2)–16 (1) dorsal and 15 (2)–16 (1) ventral, located posterior to vertebra PU_6. Posteriormost one (1) or two (2) dorsal and three or four ventral procurrent caudal-fin rays segmented. Caudal skeleton PH + 1 + 2,3 + 4 + 5. Long epural present.

Pigmentation in alcohol: Overall ground coloration light brown. Minute and numerous melanophores clustered at humeral region, forming posteriorly a midlateral stripe extending to caudal-fin base. Dark streak extending dorsally on surface of snout, between base of maxillary barbel and anterior margin of eye. Conspicuous and wide pale band at posterior margin of head, between dorsal corners of branchial openings. Pale triangular spot at dorsal-fin origin. Pale spot at adipose-fin origin variably present. Cheeks lighter than remaining surface of head. Basal portion of maxillary barbel with chromatophores on dorsal surface. Base of dorsal fin with a dark band along sides. Base of caudal fin with denser vertical cluster of chromatophores. Ventral surface of head and body pale. Interradial membrane of fins and adipose fin hyaline.

Distribution: This species is present in the Anchique, Prado, Saldaña, Coello, Totare, and Sabandija rivers, all direct tributaries of the upper Magdalena River basin (Fig. 4).

Habitat and ecological notes: Magdalenichthys poira is found in small streams of 0.1–2 m depth, substrate of sand, pebbles, and rocks, moderate current, and margins with riparian vegetation. Main food items found in dissected specimens for clearing and staining were Chironomidae, Hydropsychidae, and Ephemeroptera. This species is found syntopically in the Alvarado River with *Cetopsorhamdia molinae*, *Pimelodella floridablancaensis* Ardila Rodríguez, 2017, *Rhamdia guatemalensis* (Günther, 1864), *Pimelodus yuma* Villa-Navarro & Acero P., 2017, *Trichomycterus banneaui* (Eigenmann, 1912), *Trichomycterus mogotensis* Ardila Rodríguez, 2017, *Trichomycterus transandianus* (Steindachner, 1915), *Chaetostoma milesi* Fowler, 1941, *Chaetostoma thomsoni* Regan, 1904, *Lasiancistrus volcanensis* Dahl, 1942, *Sturisomatichthys leightoni* (Regan, 1912), *Astroblepus marmoratus* (Regan, 1904), *Astroblepus homodon* (Regan, 1904), *Sternopygus aequilabiatus* (Humboldt, 1805), *Apteronotus eschmeyeri* de Santana, Maldonado-Ocampo, Severi & Mendez, 2004, *Cynodonichthys magdalenae* (Eigenmann & Henn, 1916), *Poecilia reticulata* Peters, 1859, *Poecilia sphenops* Valenciennes, 1846, *Andinoacara latifrons* (Steindachner, 1878), *Geophagus steindachneri* Eigenmann & Hildebrand, 1910, and *Kronoheros umbrifer* (Meek & Hildebrand, 1913) (Albornoz-Garzón *et al.* 2020).

Etymology: The name poira is the most important indigenous mythological figure of the Tolima department and refers to the mischievous and libertine Mohán, who is a human-like being (when it appears in the form of a child or adolescent), with a face tanned by the sun, and penetrating and rougish eyes. The poira enchants and attracts young women, who often go to wash clothes on the banks of the river. Used as a noun in apposition.

Magdalenichthys yariguies **DoNascimiento, Albornoz-Garzón, Méndez-López, Villa-Navarro & Conde-Saldaña sp. nov.**

(Figs 9–10; Table 1)

ZooBank registration: urn:lsid:zoobank.org:act:EF13BC97-59E8-4388-82E5-58E0F825927E.

Figure 9. Left lateral, dorsal, and ventral views of *Magdalenichthys yariguies*, IAvH-P 22481, holotype, 67.9 mm SL; Santander, El Carmen de Chucurí, quebrada La Concordia, río La Colorada drainage, Magdalena River. Scale bar = 1 cm.

Holotype: IAvH-P 22481 (67.9 mm SL), Colombia, Santander, El Carmen de Chucurí, quebrada La Concordia, río La Colorada drainage, 06°34'55.2"N 73°35'36"W, 683 m a.s.l.; J.G. Albornoz-Garzón, A. Suárez-Gamboa & G. Caballero, 24 Feb 2018.

Paratypes: Santander: El Carmen de Chucurí: IAvH-P 17732 (1, 41.9 mm SL, 1 c&s, 46.8 mm SL); same locality and collectors as holotype, 22 Feb 2018. IAvH-P 17744 (2, 40.3–45.8 mm SL, 1 c&s, 53.3 mm SL); same locality and collectors as holotype, 23 Feb 2018. IAvH-P 17757 (1, 62 mm SL); collected with holotype. IAvH-P 17769 (1, 53.5 mm SL); quebrada La Concordia, río La Colorada drainage, 06°35'17.7"N 73°35'04.8"W, 672 m a.s.l.; J.G. Albornoz-Garzón & G. Caballero, 25 Feb 2018. IAvH-P 17792 (1, 60.6 mm SL); quebrada La Leona, río La Colorada drainage, 06°34'35.7"N 73°34'30.7"W, 713 m a.s.l.; J.G. Albornoz-Garzón, 26 Feb 2018.

Diagnosis: Magdalenichthys yariguies can be distinguished from all its congeners by having 40 vertebrae (vs. 36–37 in *M. lundbergi*, 32–33 in *M. mompox*, 38–39 in *M. poira*); more principal (segmented) anal-fin rays (11–12 vs. 9–10); and last anal-fin pterygiophore anterior to hemal spine of vertebrae 33–34 (vs. 29–30 in *M. lundbergi*, 30 in *M. poira*, 27 in *M. mompox*). *Magdalenichthys yariguies* is distinguished from *M. lundbergi* and *M. mompox* by having a longer anal-fin base (15.6–18.1% of SL vs. 11.7–14.4% in *M. lundbergi*, 9.9–13.5% in *M. mompox*). *Magdalenichthys yariguies* is distinguished from *M. lundbergi* and *M. poira* by having the adipose-fin origin posterior to the anal-fin origin (vs. at same vertical). *Magdalenichthys yariguies* is distinguished from *M. mompox* and *M. poira* by number of gill rakers on first arch (3–4 vs. 7–8 in *M. mompox*, 5–6 in *M. poira*); first dorsal-fin pterygiophore inserted posterior to neural spine of vertebra 12 (vs. vertebra 9 in *M. mompox*, vertebrae 10–11 in *M. poira*); more anal-fin pterygiophores (11 vs. 9–10); and fewer branched rays in the upper lobe of the caudal fin (six vs. seven). *Magdalenichthys yariguies* further differs from *M. lundbergi* by having fewer rows of dentary teeth (four vs. five or more); shorter caudal peduncle (16.3–19.3% of SL vs. 20.1–24.2%); and longer maxillary barbel (24.2–30.9% of HL vs. 17.5–23%). *Magdalenichthys yariguies* further differs from *M. mompox* by having a parabolic contour of the head in dorsal view, with lateral profiles convex (vs. rectangular, with lateral profiles straight); first anal-fin pterygiophore inserted posterior to hemal spine of vertebrae 24–25 (vs. vertebra 21); upper-caudal fin lobe distinctively longer than lower lobe (vs. both lobes subequal); fewer caudal-fin branched rays (13 or fewer vs. 15); narrower cleithral width (12.8–15.2% of SL vs. 15.3–19.1%); longer adipose-fin base (26.2–28.9% of SL vs. 17.5–20.9%); shorter prepelvic distance (35.4–41.5% of SL vs. 42–47.9%); shorter caudal-fin lower lobe (16.3–19.4% of SL vs. 21.9–24.9%); and shorter head (16.7–20.4% of SL vs. 22.9–25.1%). *Magdalenichthys yariguies* further differs from *M. poira* by having more branched pectoral-fin rays (eight vs. seven); fewer dorsal procurrent caudal-fin rays (13 vs. 14–16); fewer ventral procurrent caudal-fin rays (13–14 vs. 15–16); smaller eye (7.0–11.7% of HL vs. 11.9–17.8%); and narrower mouth (35.4–41.8% of HL vs. 41.3–53.5%).

Description: Morphometric data in Table 1. Refer to Figure 9 for general appearance. Small heptapterine catfish (largest specimen 67.9 mm SL), with elongated body, elliptical in cross-section at dorsal-fin origin (longest axis horizontal), progressively more compressed to caudal region. Dorsal profile slightly convex from snout tip to occipital region, straight immediately posterior from this point to adipose-fin origin, sloping ventrally along adipose-fin

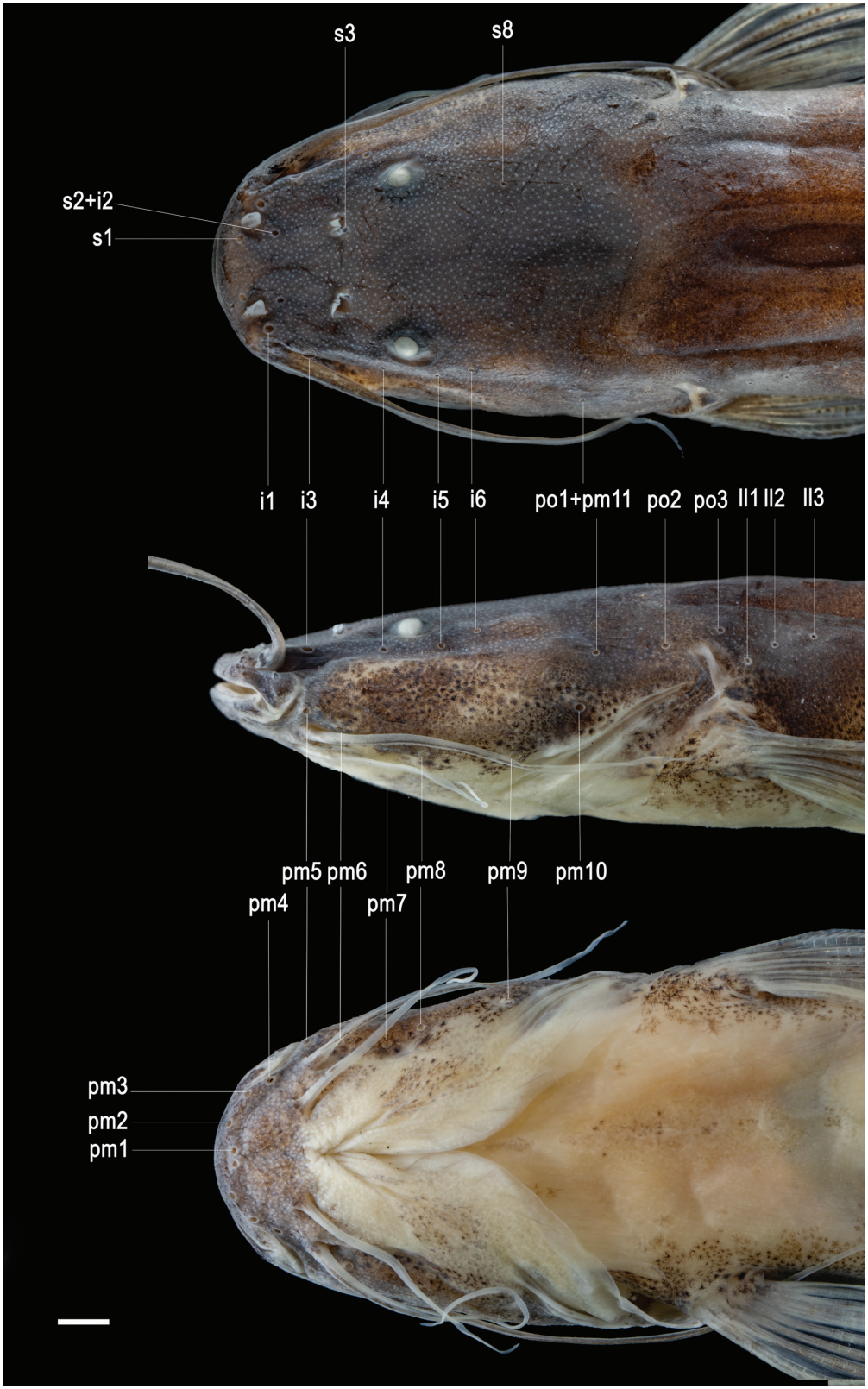

Figure 10 . Dorsal, lateral, and ventral views of head, showing cephalic laterosensory pores in *Magdalenichthys yariguies*, paratype, IAvH-P 17744, 45.8 mm SL. Abbreviations: i, infraorbital; pm, preoperculo-mandibular; po, postotic; s, supraorbital; ll, lateral line. Scale bar = 1 mm.

base, and slightly ascending along dorsal membrane supported by procurrent caudal-fin rays. Ventral profile of head slightly convex, then straight to pelvic-fin insertion, slightly concave from this point to anal-fin origin, ascending along anal-fin base to origin of procurrent caudal-fin rays and slightly descending along ventral membrane supported by procurrent caudal-fin rays.

Head depressed, parabolic in dorsal view, dorsally covered by thin skin. Cheek filled with muscular mass of adductor

mandibulae, but muscle not reaching dorsally onto skull roof. Snout short and rounded. Mouth slightly prognathous. Premaxillary teeth arranged in a rhomboidal patch of 4–5* medial and eight lateral irregular rows of minute conical teeth. Lower jaw slightly longer than upper jaw. Dentary teeth arranged in four irregular rows of minute conical teeth, similar to those on premaxilla. Maxillary barbel reaching distal tip of innermost pectoral-fin ray. Conspicuous groove accommodating anterior part of maxillary barbel along sides of head, delimiting dorsal and lateral regions of head. Bases of outer and inner mental barbels in a straight line. Outer mental barbel reaching pectoral-fin base. Inner mental barbel surpassing branchial opening. Subcutaneous eye small, dorsal in position and slightly longer in horizontal than vertical axis. Anterior naris tubular. Posterior naris closer to anterior margin of eye than to anterior naris, anteriorly bordered by a low fleshy margin. Anterior and posterior internarial widths equal. Nares disposed in a squared arrangement. Branchiostegal membrane free, supported by eight rays and joined to isthmus only at anteriormost point. Gill rakers on first arch 3–4, located along anterior margin of ceratobranchial.

Lateral line canal complete, reaching caudal skeleton. Supraorbital pore s1 medially adjacent to anterior naris; s2 + i2 pore slightly closer to anterior naris (Fig. 10), at end of posteriorly directed membranous tubule, originating from commissure connecting supraorbital and infraorbital canals, closer to supraorbital canal; s3 pore inside posterior naris, adjacent to its posterior margin, at notch of cutaneous membrane. Contralateral supraorbital canals connected medially by epiphyseal membranous branch, dorsal to middle of anterior fontanel, without superficial pore; s8 pore (parietal branch) arising from a posteriorly directed membranous canal, externally located posterior to eye, at level of medial margin of eye; s4 and s7 branches and pores absent. Infraorbital pore i1 laterally adjacent to anterior naris, between naris and maxillary barbel base; i3 pore posterior to maxillary barbel base; i4 pore at vertical through anterior margin of eye; i5 pore behind vertical through posterior margin of eye; i6 pore posterior to eye, aligned with ventral margin of eye. Pterotic branch (po2) at posterolateral corner of pterotic. Dentary with seven pores of preoperculo-mandibular canal. Submental pores (pm1) paired. Sixth and seventh mandibular pores approximately at same vertical level. Subpreopercular ossicle with one pore (pm8). Preopercle with two pores, anterior pore (pm9) originating from membranous tubule lateral to interopercle and posterior pore (pm10) from membranous tubule passing lateral to ventral portion of opercle. Last preopercular pore (po1 + pm11) at end of membranous tubule, dorsal to dorsoposterior portion of opercle. Axillary branch (ll1) ventral, running posterior to supracleithrum.

Precaudal vertebrae 11 (1)–12 (1), thoracic vertebrae 9, and caudal vertebrae 28 (1)–29 (1), totalling 40 vertebrae. Ribs seven or eight (last pair shortest). Pectoral fin with i,8 rays. First pectoral-fin ray (unbranched) soft and shorter than first branched ray. First branched ray longest. Distal margin of pectoral fin convex. Pelvic fin with i,5 rays. First pelvic-fin ray (unbranched) thick and shortest, second and third branched rays longest. Pelvic-fin origin opposite to dorsal-fin origin, at vertical through vertebra 14 or 15. Dorsal fin lacking spinelet, with one unbranched and six branched rays, supported by seven pterygiophores. Dorsal-fin margin convex, its unbranched ray slightly shorter than first branched ray; first three branched rays subequal. First dorsal-fin pterygiophore inserted posterior to neural spine of vertebra 12 and last pterygiophore anterior to neural spine of vertebra 17. Adipose fin long, almost rectangular with attenuated ends and posterior lobe free. Adipose-fin origin at vertical through second unbranched ray of anal fin. Anal fin with 2–3 procurrent (unsegmented) rays, and 3* (5)–4 (2) unbranched and 8* (6)–9 (2) branched rays for a total of 11 (5) or 12 (3) principal rays. Anal-fin distal margin rounded. Anal fin supported by 11 pterygiophores. First anal-fin pterygiophore posterior to hemal spine of vertebrae 24 (1)–25 (1) and last pterygiophore anterior to hemal spine of vertebrae 33 (1)–34 (1). Caudal fin deeply forked with i,6 + 7,i* principal rays (one c&s specimen with six branched rays in the lower lobe). Upper lobe of caudal fin conspicuously longer than lower lobe, both lobes pointed. Procurrent caudal-fin rays 13 dorsal and 13–14 ventral, located posterior to vertebrae PU_6. Posteriormost four procurrent caudal-fin rays segmented. Caudal skeleton PH + 1 + 2,3 + 4 + 5. Long epural present.

Pigmentation in alcohol: Overall ground coloration marbled. Minute and numerous melanophores clustered at humeral region, forming posteriorly a midlateral inconspicuous stripe extending to caudal-fin base. Myosepta delineated by chromatophores, more evident above anal-fin base. Dorsal surface of head and predorsal area darker than remaining surface of body. Dark streak extending dorsally on surface of snout, between base of maxillary barbel and anterior margin of eye. Conspicuous and narrow pale band with roughly M-shaped, posterior to head, between dorsal corners of branchial openings. Cheeks and maxillary groove lighter than remaining surface of head, peppered with sparse chromatophores. Basal portion of maxillary barbel darkly pigmented on dorsal surface. Base of dorsal fin with a dark band along sides. Ventral surface of head with anterior crescent shaped dusky area fading posteriorly, isthmus and branquiostegal membrane pale. Abdomen pale, sparse chromatophores posterior to ventral fins. Adipose fin with marbled pattern of chromatophores. Dorsal-fin rays with chromatophores. Basal portion of pectoral and pelvic-fin rays with chromatophores. Base of anal-fin rays with chromatophores. Caudal-fin rays with minute chromatophores, giving diffuse dark pigmentation. Interradial membrane of fins hyaline.

Distribution: This species is restricted to the La Colorada River drainage, a direct tributary of the middle section of the Magdalena River basin (Fig. 4).

Habitat and ecological notes: The type locality of *Magdalenichthys yariguies* is a stream with an average width of 7 m, substrate of sand, pebbles, and rocks, and margins with abundant riparian vegetation (Fig. 11). Specimens of *M. yariguies* were found syntopically with *Hoplias malabaricus* (Bloch, 1794), *Lebiasina floridablancaensis* Ardila Rodríguez, 2001, *Astyanax yariguies* (Torres-Mejia, Hernández & Senechal, 2012), *Creagrutus guanes* Torres-Mejia & Vari, 2005, *Creagrutus magdalenae* Eigenmann, 1913, *Hemibrycon plutarcoi* (Román-Valencia, 2001), *Hemibrycon* sp., *Knodus* sp., *Trichomycterus*

Figure 11. Type locality of *Magdalenichthys yariguies*. Colombia, Santander, Magdalena River, El Carmen de Chucurí, río Cascajales drainage, quebrada La Concordia. Photograph by M. Arias-Mañosca.

calai Ardila Rodríguez, 2019, *Trichomycterus* cf. *transandianus* (Steindachner, 1915), *Trichomycterus* sp., *Astroblepus* cf. *verai* Ardila Rodríguez, 2015, *Farlowella yarigui* Ballen & Mojica, 2014, *Dolichancistrus carnegiei* (Eigenmann, 1916), *Lasiancistrus volcanensis* Dahl, 1941, *Pimelodella floridablancaensis*, *Poecilia caucana* (Steindachner, 1880), and *Geophagus steindachneri*.

Etymology: The name yariguies honours the exterminated indigenous group that inhabited the río Cascajales drainage. Used as a noun in apposition.

DNA barcode species delimitation

We analyzed DNA barcode sequences for 19 specimens of *Magdalenichthys* from different localities along the Magdalena River basin (Supporting Information, Table S1). Stop codons, deletions, or insertions were absent in all sequences. After aligning and editing, the final matrix had 603 base pairs (bp) with a total of 513 sites (excluding missing data), of which 404 were conserved and 109 were variable. Base composition was 25.1% adenine, 27.4% cytosine, 17.6% guanine, 27.2% thymine, and 2.8% missing data. The substitution saturation test revealed Index of Substitution Saturation values lower than symmetrical (balanced) tree topologies (Iss.cSym) and asymmetrical (unbalanced) tree topologies (Iss.cAsym) values, which indicates the lack of saturation signal in the matrix.

Species delimitation using three methods, incorporating both distance and tree-based techniques, yielded similar results. The PTP and ASAP methods returned identical results, delimiting four species of *Magdalenichthys*; however, the GMYC delimited only three groups, merging in a single group, *M. lundbergi* and *M. poira* (Fig. 12).

The genetic distance analysis also supported recognition of the four species of *Magdalenichthys*. The analysis showed low intraspecific genetic variation (< 0.11 ± 0.11%) and pairwise interspecific distances higher than 3%, ranging from 3.0 ± 0.7% between *M. lundbergi* and *M. poira* to 5.0 ± 1.0% between *M. yariguies* and *M. mompox* (Table 2).

Phylogenetic relationships

Sequencing and data filtering yielded an initial edge-trimmed aligned matrix comprising 697 492 bp and 2443 UCE loci for 78 specimens (59 heptapterid and 19 outgroup taxa). The total matrix included 33 133 908 characters, of which 26 499 164 were nucleotides and 6 634 744 (20%) were missing data. Mean locus length after alignment and trimming was 286 nucleotides (range: 101–3366). The size of the final matrix according to its completeness level (70%) was 1069 loci containing 310 338 bp.

The three methods used (i.e. BI, ML, ASTRAL-III) recovered nearly identical topologies and strong node support. The BI and ML analyses returned identical topologies, the phylogeny in Figure 13 corresponds to the results of the BI analysis. The coalescent-based tree (ASTRAL-III) is presented in Supporting Information, Figure S1. The phylogenomic analyses recovered with highest confidence (BI PP = 1, 100% ML bootstrap, ASTRAL PP = 1) the placement of *Magdalenichthys*, represented by *M. lundbergi* and *M. poira*, as sister to *Phenacorhamdia* (Fig. 13). Accordingly, *Magdalenichthys* is resolved within the clade 3 of Heptapterini (Silva *et al.* 2021), consisting of *Cetopsorhamdia* + (*Pariolius* Cope, 1872 + (*Magdalenichthys* + *Phenacorhamdia*)).

DISCUSSION

The family Heptapteridae stands out as one of the most species-rich groups of catfishes in the Neotropics; however, its taxonomic inventory has lagged behind that of the other two most speciose Neotropical siluriform families, i.e. Loricariidae and Trichomycteridae. The number of new species added to

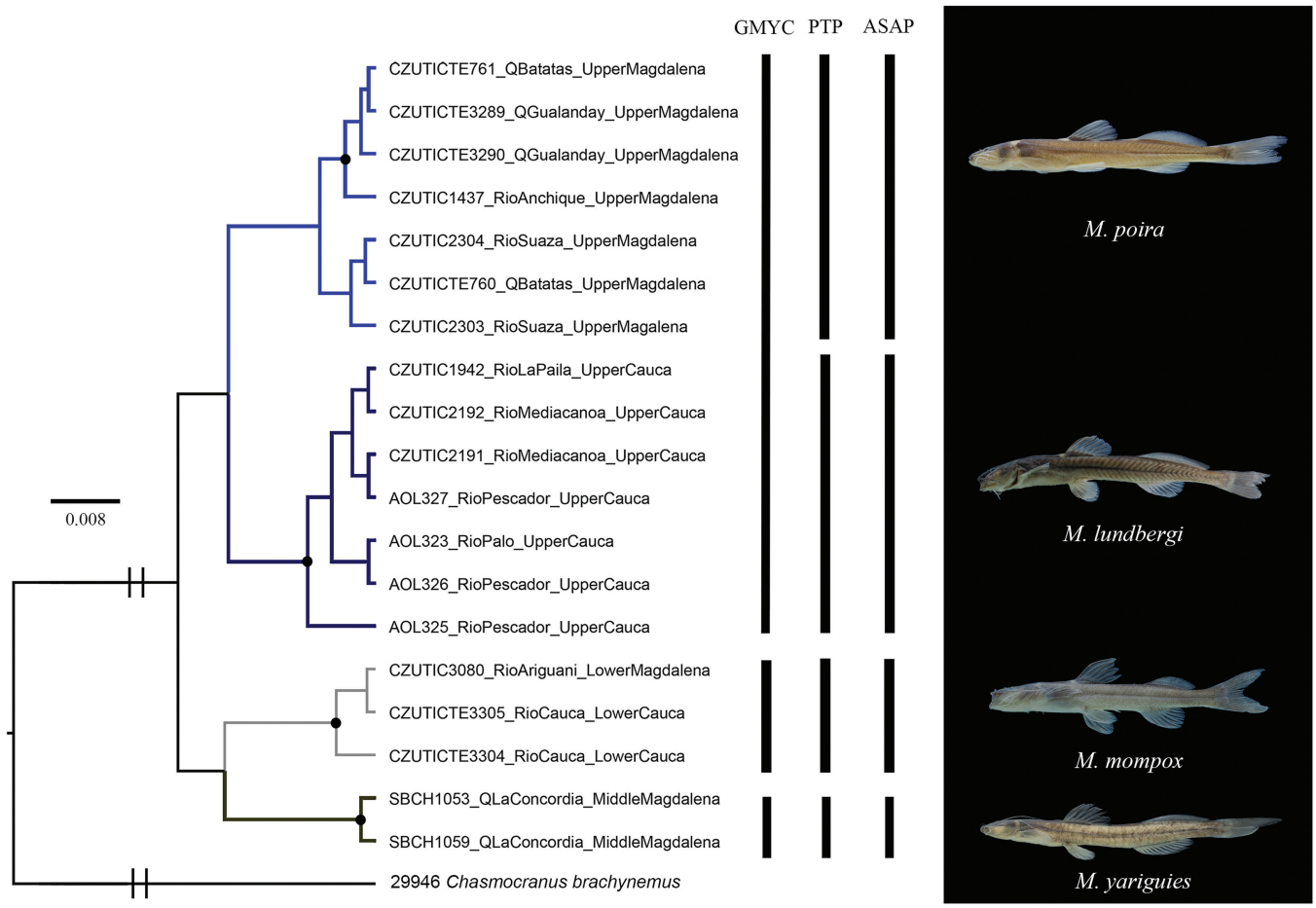

Figure 12. Bayesian phylogenetic *COI*-tree representing species delimitation analyses of *Magdalenichthys*. The black dots in the node branches represent posterior probabilities greater than 0.95.

Table 2. Parwise TN93 genetic distance and standard error values (given in percentage), among species of *Magdalenichthys*. Bold numbers represent intraspecific genetic variation

	M. poira	*M. mompox*	*M. yariguies*	*M. lundbergi*
M. poira	**0.1 ± 0.1**			
M. mompox	3.3 ± 0.7	**0.1 ± 0.1**		
M. yariguies	4.7 ± 0.9	5.0 ± 1.0	**0.0 ± 0.0**	
M. lundbergi	3.0 ± 0.7	4.8 ± 0.9	4.6 ± 0.9	**0.0 ± 0.0**

Heptapteridae in the past decade has been a modest number of just 25 species, which is a small number when compared to the new species of loricariids (194 spp.) and trichomycterids (149 spp.) documented from the same period (Fricke *et al.* 2024). Similarly, for more than two decades, since the still unpublished dissertation of Bockmann (1998), no major contributions to the phylogenetic knowledge of the family were added, until the recent publication of two molecular studies (Faustino-Fuster *et al.* 2021, Silva *et al.* 2021), mainly providing resolution to the internal relationships of the supragenetic lineages that constitute Heptapteridae: Rhamdiinae and Heptapterinae (composed of Brachyglaniini and Heptapterini). Nonetheless, the systematic resolution and taxonomic delimitation of most heptapterid genera is still a problem to be addressed. This scenario has obviously resulted in the paucity of taxonomic contributions on the heptapterid fauna from Colombia, with only six species described and five new records added to the country checklist in the past two decades (DoNascimiento *et al.* 2023). *Magdalenichthys* remained ignored for almost 20 years and surprisingly, a single species was only suspected to be part of this genus, despite the great morphological variation exhibited by the species herein described, from rather elongated forms such as *M. lundbergi*, *M. poira*, and its extreme end in *M. yariguies* with 40 vertebrae, to short-bodied forms as *M. mompox*, with only 32–33 vertebrae, with this latter species even resembling *Phenacorhamdia taphorni* DoNascimiento & Milani, 2008, a species of the 'long snout and short body' group proposed by Bockmann (1998) for *Phenacorhamdia*.

Formerly, *Magdalenichthys* was recorded in Colombian fish collections under the taxonomic identity of *Heptapterus panamensis* (Bussing, 1970), an unquestionably similar looking species at first sight, showing an elongate body, rectangular adipose fin, and upper caudal-fin lobe longer that the lower lobe. However, careful comparison of both taxa reveals obvious differences even in their external appearance: prognathous mouth in *Magdalenichthys* (vs. terminal in *H. panamensis*) and more anterior insertion of pelvic fin in *Magdalenichthys* (anterior to middle of dorsal-fin base vs. at middle of dorsal-fin base in *H. panamensis*). In addition, *H. panamensis* lacks the exclusive

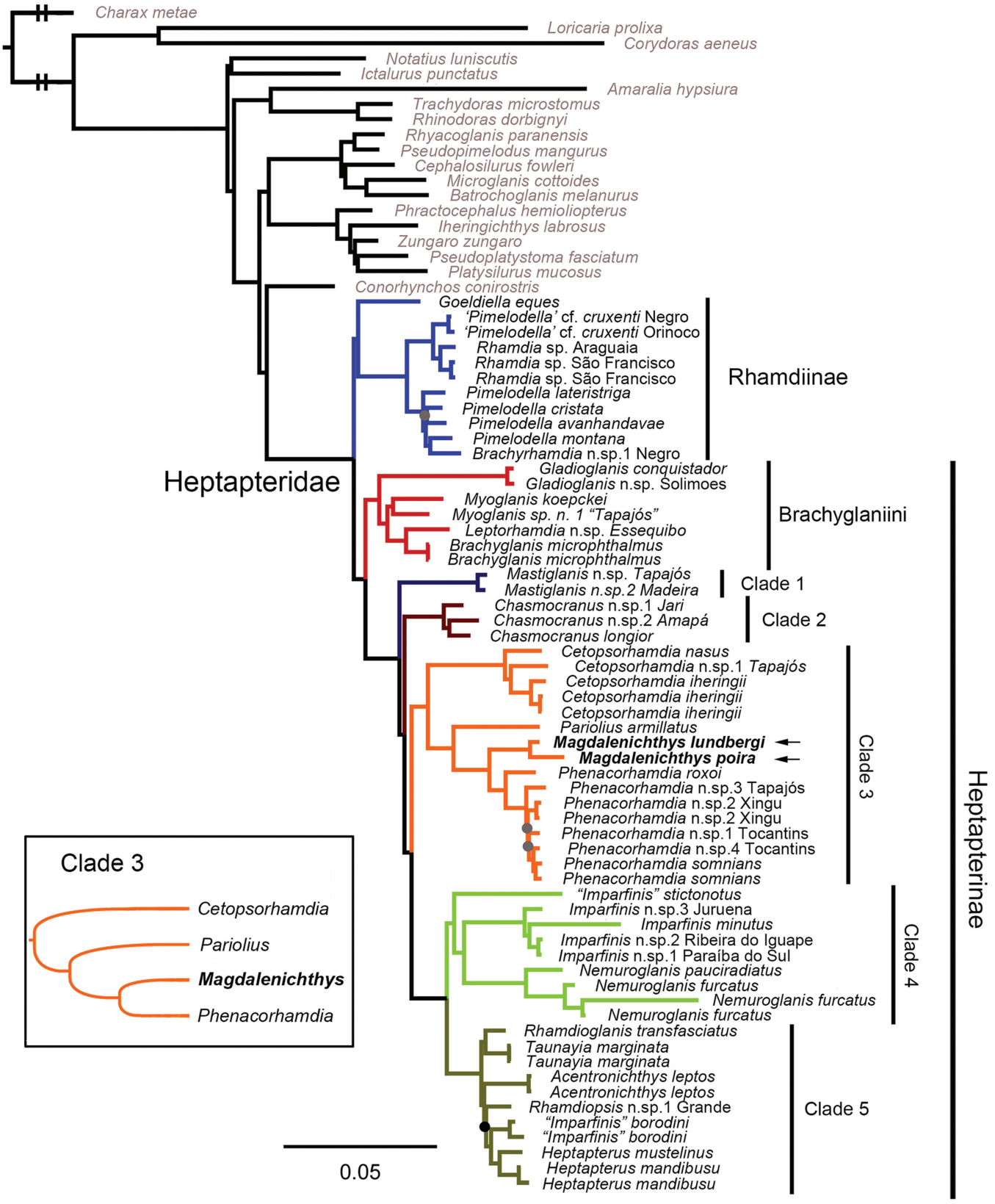

Figure 13. Phylogenetic relationships of *Magdalenichthys* within Heptapteridae obtained from a concatenated alignment of 1069 UCE loci based on Bayesian analysis of 70% complete, edge-trimmed, unpartitioned data. All heptapterid nodes supported Bayesian posterior probabilities > 0.99 and bootstrap values > 99%, except a black dot that denote a single node with bootstrap = 96%, and grey dots that denote nodes with bootstrap values between 60% and 80%.

autapomorphy defining monophyly of *Magdalenichthys*, i.e. pointed posterior process of lateral ethmoid adjacent to lateral margin of neurocranium. Otherwise, *Magdalenichthys* also lacks a putative derived character exclusively present in *H. panamensis* and an undescribed species from northern Venezuela, consisting of paired anterodorsal laminar processes extending beyond the articular cartilage of the dorsal arm of the quadrate, enclosing anteriorly and posteriorly the metapterygoid, at its articulation with the quadrate. Some heptapterid genera (e.g. *Chasmocranus*, *Phenacorhamdia*) only show the anterior extension of the quadrate, but the posterior process is always missing, being the margin of the dorsal arm of the quadrate, immediately posterior to the articular block, straight and continuous with the cartilage margin. *Heptapterus panamensis* was initially hypothesized by Bockmann (1998) as a member of a clade equivalent in composition to the clade 3 of Silva *et al.* (2021), differing the composition of this clade in both works by the mutual inclusion/exclusion of *Chasmocranus/Cetopsorhamdia* in the former, and *Cetopsorhamdia/Chasmocranus* in the latter. Although, it is worth mentioning that partially congruent results with Bockmann's hypothesis were reached by Faustino-Fuster *et al.* (2021), showing *Chasmocranus* as a member of this clade as sister to the whole group, which includes at the same time *Cetopsorhamdia*, as the next successive sister group to the remainder of the clade. Exploratory phylogenetic analyses with available *COI* sequences of *Heptapterus panamensis* from public repositories (either sequences from other markers or tissue samples were not available for our study) reveal that this species is nested in a different clade from that including the sister pair *Magdalenichthys* + *Phenacorhamdia* (Supporting Information, Fig. S2), corroborating our morphological findings dismissing the membership of *H. panamensis* in *Magdalenichthys*. On the other hand, *H. panamensis* has been recorded in Colombia, but only from the lower basin of the Atrato River (Maldonado-Ocampo *et al.* 2006), an independent Caribbean versant river basin draining west of the Magdalena basin.

The consistent recovery of the sister group relationship of *Magdalenichthys* and *Phenacorhamdia* in our phylogenetic analyses using different molecular markers, UCEs (Fig. 13), and *COI* (Supporting Information, Fig. S2) is further supported by at least two apomorphic shared conditions, (i) a prognathous mouth, a character originally proposed as diagnostic for *Phenacorhamdia*, being now interpreted as exclusively shared with *Magdalenichthys* within Heptapterini, and (ii) presence of a well-developed posterior process on the epioccipital, delimiting posteriorly the ascending process of the supracleithrum (Fig. 14), granting that this last condition is not exclusive within the family and occurs homoplastically (based on our UCE topology) at least in *Rhamdiopsis* (Bockmann and Castro 2010: fig. 4a, p. 683).

Magdalenichthys poira (Fig. 15D) and *M. yariguies* (Fig. 15E) show an osseous bridge connecting the anterior and posterior branches of the transverse process of the fourth vertebra, while this bridge is lacking in *M. lundbergi* (Fig. 15B) and *M. mompox* (Fig. 15C). At least, *Phenacorhamdia anisura* also has both branches connected by the osseus bridge as shown in Figure 15A, but apparently there is also interspecific variation within this genus (illustrated as absent in Bockmann 1998: fig. 168, p. 547). This character has been proposed as synapomorphic for a subset of species of *Rhamdella* (Bockmann and Miquelarena 2008) and as an autapomorphy for *Rhamdiopsis krugi* (Bockmann and Castro 2010), but its homoplastic distribution extends to *Heptapterus carnatus* (Faustino-Fuster *et al.* 2019: figs 4b–c, p. 359), although showing asymmetric presence. Phylogenetic significance of this character for the sister group relationship of *Magdalenichthys* and *Phenacorhamdia* remains to be assessed in a more encompassing sampling of the latter genus.

Regarding morphological support within the clade 3 of Silva *et al.* (2021), *Magdalenichthys*, *Pariolius*, and *Phenacorhamdia* share a derived condition of the cephalic laterosensory canal, consisting in the loss of the sensory pore of the epiphyseal branch (s6) (Figs 3, 6, 8, 10). Plesiomophically, epiphyseal branches (either medially fused or not) have sensory pores in heptapterids and siluriforms in general. *Magdalenichthys* and *Pariolius* also show an apomorphic slender ascending portion of the Meckel's cartilage, anterodorsally directed, forming an acute angle with the horizontal portion (Fig. 16). In the plesiomorphic condition (present in *Cetopsorhamdia nasus*), the ascending portion of the Meckel's cartilage is of similar width to the horizontal portion or if slender, is always vertically oriented at a right angle in relation to the horizontal portion of the cartilage (Ortega-Lara 2012: fig. 9, p. 59). This

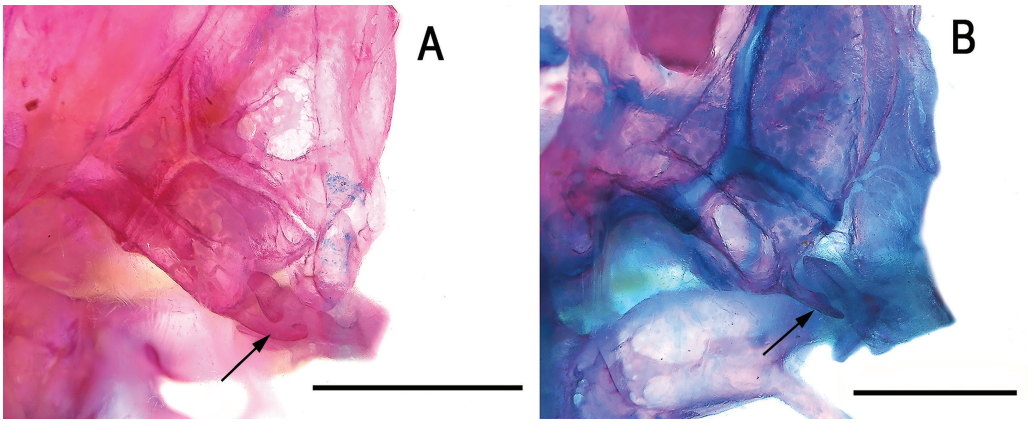

Figure 14. Dorsal view of occipital region of (A) *Phenacorhamdia anisura*, IAvH-P 7932, 41 mm SL and (B) *Magdalenichthys yariguies*, paratype, IAvH-P 17732, 46.8 mm SL. Arrows indicate epioccipital process. Scale bar = 1 mm.

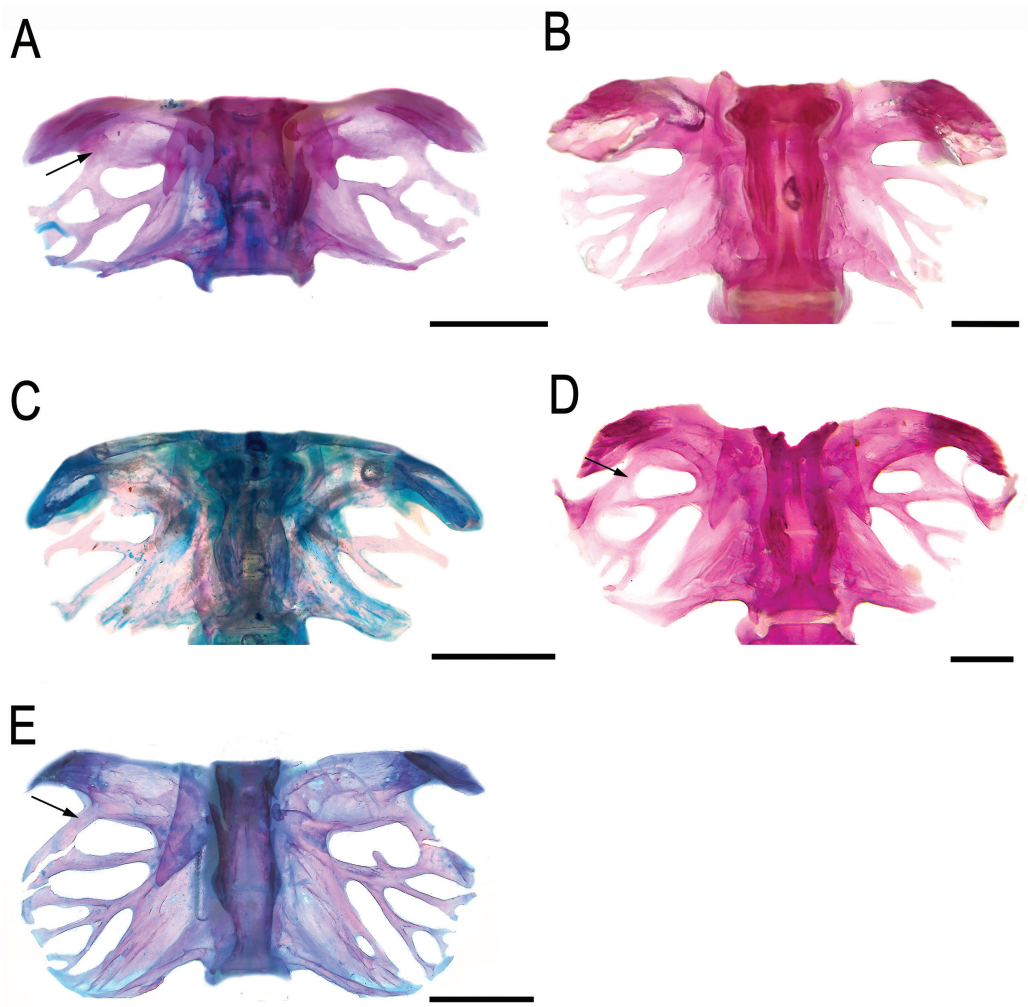

Figure 15. Ventral view of Weberian complex of (A) *Phenacorhamdia anisura*, IAvH-P 7932, 41 mm SL; (B) *Magdalenichthys lundbergi*, paratype, IMCN 3506, 87.1 mm SL; (C) *Magdalenichthys mompox*, paratype, CZUT-IC 20495, 33.4 mm SL; (D) *Magdalenichthys poira*, paratype, CZUT-IC 8624, 44.7 mm SL; (E) *Magdalenichthys yariguies*, paratype, IAvH-P 17732, 46.8 mm SL. Arrows indicate osseous bridge joining anterior and posterior branches of transverse process 4. Scale bars = 1 mm.

derived character-state could be interpreted as potentially informative for a more encompassing group, including at least *Magdalenichthys*, *Pariolius*, and *Phenacorhamdia*. However, the condition present in *Phenacorhamdia* is not comparable, given that its ascending process of Meckel's cartilage is reduced to a small cartilaginous nodule, isolated from the main horizontal portion of the cartilage. This last condition, which is also interpreted as apomorphic, is conspicuously present in *Imparfinis microps* Eigenmann & Fisher, 1916, also included by Bockmann (1998) in the same clade of *Pariolius* and *Phenacorhamdia*, thus hindering a straightforward interpretation of character-state transitions for the ascending portion of Meckel's cartilage, provisionally based on our admittedly taxonomically incomplete UCE phylogenetic analysis, therefore requiring a quantitative analysis to properly assess its optimization.

Based on variation gaps in characters of the external and internal morphology, supplemented by molecular species delimitation analyses based on the *COI* marker, we recognized four mitochondrial lineages defined here as distinct species within *Magdalenichthys*. These species can be easily differentiated morphologically by a series of morphometric, meristic, discrete, and pigmentation attributes. The species delimitation methods PTP and ASAP yielded identical results, supporting the recognition of the four species. These results were partially consistent with the GMYC method, which clustered in a single operational taxonomic unit (OTU), *M. lundbergi* and *M. poira*. However, the interspecific genetic distances between these two species was 3%, larger than the 2% heuristic intraspecific cut-off value proposed to delimit Neotropical freshwater fish species (Hebert *et al.* 2003, Pereira *et al.* 2013, Pugedo *et al.* 2016). Although some studies using the GMYC approach have reported results with lineage over-splitting (Miralles and Vences 2013, Paz and Crawford 2012), where usually the number of entities recovered exceeds the total number of morphospecies represented in the datasets (Talavera *et al.* 2013), GMYC can also result in an underestimation of the number of species, depending on different models of ultrametric branch length optimization (i.e. coalescent models) (Hendrich *et al.* 2010), as well as the result of the influence of either recent gene flow, recent radiations, or when ancestral polymorphism is extremely high

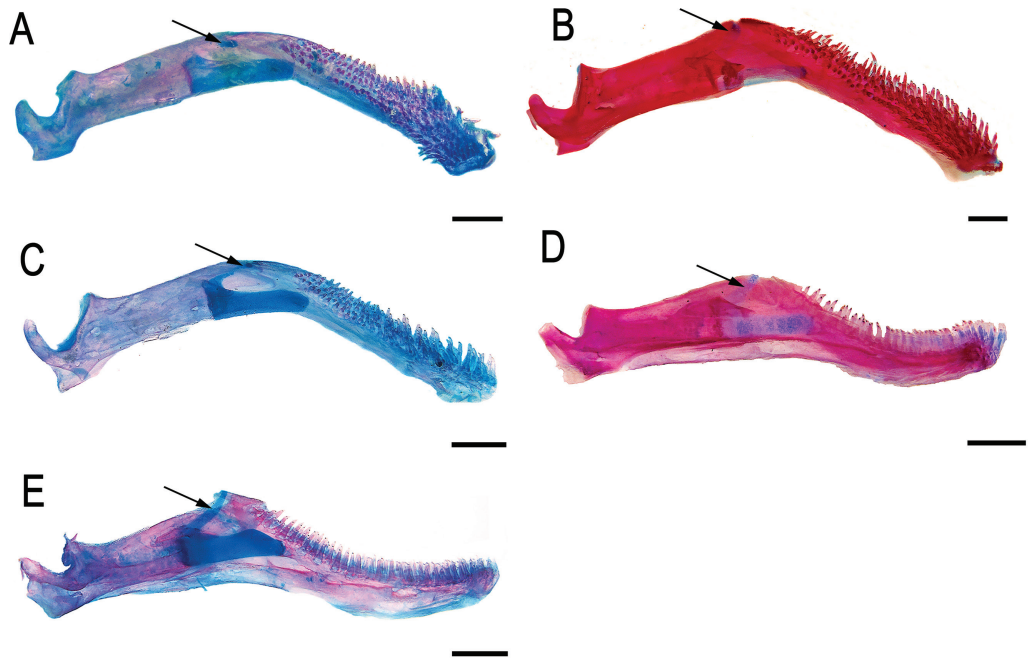

Figure 16. Medial view of left lower jaw of (A) *Phenacorhamdia anisura*, IAvH-P 7932, 41 mm SL; (B) *Magdalenichthys lundbergi*, paratype, IMCN 3506, 87.1 mm SL; (C) *Magdalenichthys mompox*, paratype, CZUT-IC 20495, 33.4 mm SL; (D) *Magdalenichthys poira*, paratype, CZUT-IC 8624, 44.7 mm SL; (E) *Magdalenichthys yariguies*, paratype, IAvH-P 17732, 46.8 mm SL. Arrows indicate ascending portion of Meckel's cartilage. Scale bars = 1 mm.

(Esselstyn *et al.* 2012, Wade *et al.* 2015). Considering the consistency between the PTP and ASAP methods, the genetic distances approach, and the morphological disparity found in the *Magdalenichthys* OTUs, we concluded that our GMYC results underestimated the actual diversity of this catfish genus.

The distributions of *Magdalenichthys* species are concordant with the geography and geological characteristics of the Magdalena basin in the northern Andes. The restricted distribution of *M. lundbergi* to the upper basin of the Cauca River corresponds with a long-recognized pattern of endemism in this region (Ortega-Lara *et al.* 2006, Villa-Navarro *et al.* 2017, Martínez *et al.* 2022); some examples of endemic species are found in other Heptapteridae [*Pimelodella macrocephala* (Miles, 1943): Usma-Oviedo and Ortega-Lara 2012; *Cetopsorhamdia boquillae*: Ortega-Lara 2022], and also in Pimelodidae (*Pimelodus crypticus*: Villa-Navarro *et al.* 2017), Loricariidae (*Lasiancistrus caucanus* Eigenmann, 1912: Poveda-Cuellar *et al.* 2023), Characidae [*Creagrutus caucanus* Eigenmann, 1913: Albornoz-Garzón *et al.* 2018; *Gephyrocharax caucanus* Eigenmann, 1912: Vanegas-Ríos 2016; *Genycharax tarpon* Eigenmann, 1912: Lehmann *et al.* 2012a; *Carlastyanax aurocaudatus* (Eigenmann, 1913): Lehmann and Usma-Oviedo 2012b], and Parodontidae (*Parodon caliensis* Boulenger, 1895: Londoño-Burbano *et al.* 2011), among others. A similar case occurs with the Serranía de Los Yariguíes, where *Astyanax yariguies* and *Farlowella yarigui* represent endemics from tributaries of this region of the middle basin of the Magdalena River (Torres-Mejía *et al.* 2012, Ballen and Mojica 2014).

The interesting pattern of diversity exhibited by *Magdalenichthys* is similar to that of other genera which are also represented by several species distributed along the Magdalena basin. Other small-size heptapterines such as *Imparfinis* and *Cetopsorhamdia* are represented by three species each in this basin (Ortega-Lara *et al.* 2011, García-Alzate *et al.* 2020). Likewise, siluriform genera such as *Pimelodus* Lacepède, 1803 (Villa-Navarro *et al.* 2017) and *Sturisomatichthys* Isbrücker & Nijssen, 1979 also have three species each in the Magdalena basin (Londoño-Burbano and Reis 2019), or even the climbing catfish *Astroblepus* Humboldt, 1805, with high rates of endemism, has several lineages along the Magdalena basin (Ochoa *et al.* 2020). However, these genera also have species distributed in the adjacent trans-Andean basins and in the cis-Andean region, unlike *Magdalenichthys*, which is so far known to be restricted to the Magdalena basin in the trans-Andean region of northern South America. This geographic pattern may imply two hypothetical scenarios: (i) emergence of this clade after high tectonic activity during the Middle Miocene (*c.* 11 Mya) in northern South America, which generated an extensive uplift of the Eastern Cordillera, fragmenting aquatic faunas of cis and trans-Andean basins (Cassemiro *et al.* 2023), or (ii) a more recent divergence, before closure of the Andean lowland portal (Montes *et al.* 2021) which connected the sedimentary Cauca-Patía basin with the western Amazon basin, followed by a relatively rapid diversification in the Magdalena basin, this last scenario being plausible, given the apparent absence of *Magdalenichthys* and *Phenacorhamdia* in the Maracaibo Lake basin, which kept a longer connection with the Orinoco basin (Lundberg *et al.* 1998, Albert *et al.* 2006, Hardman and Lundberg 2006). Future studies focused on investigating divergence times of *Magdalenichthys* will shed light on these contrasting hypotheses, and contribute to the understanding of the evolutionary history and the processes underlying the diversification of these Andean catfishes.

Comparative material: COLOMBIA: *Cetopsorhamdia orinoco*: IAvH-P 9713 (1 c&s, 35.7 mm SL); Casanare, Sabanalarga, río Upía at the bridge on the road to Sisga, Orinoco River basin, 04°49'9.4"N 73°4'57.6"W. IAvH-P 23630 (1 c&s, 36.3 mm SL); Meta, Castilla La Nueva, río Orotoy, Orinoco River basin, 03°52'08.3"N 73°38'02.3"W. *Cetopsorhamdia* sp: IAvH-P 18147 (1 c&s, 56.3 mm SL); Arauca, Tame, río Cravo Norte, Orinoco River basin, 06°30'9.3"N 71°45'55.1"W. *Gladioglanis machadoi*: IAvH-P 14578 (1 c&s, 24.4 mm SL); Vichada, La Primavera, caño Resaca, Orinoco River basin, 05°50'34.4"N 68°44'31.8"W. IAvH-P 14648 (1 c&s, 23.5 mm SL); Vichada, Puerto Carreño, caño Grande, Orinoco River basin, 05°45'52.8"N 68°23'4.4"W. *Goeldiella eques*: IAvH-P 25758 (1 c&s, 93.4 mm SL); Vichada, Puerto Carreño, laguna La Cachamera, Orinoco River basin, 05°59'36.6"N 67°25'16.6"W. *Heptapterus panamensis*: USNM 204692, holotype (61.0 mm SL); Panamá, Veraguas, creek crossing road just before entering Santa Fe. USNM 204693, paratypes, 40 (22.5–68.8 mm SL); collected with holotype. *Imparfinis microps:* IAvH-P 18990 (1 c&s, 41.8 mm SL); Cundinamarca, Medina, caño Largo, Orinoco River basin, 04°29'38.4"N 73°22'47.4"W. *Imparfinis pristos*: IAvH-P 9999 (1 c&s, 24.8 mm SL), Vichada, Cumaribo, caño Fruta, Orinoco River basin, 04°26'28.8"N 67°55'28.1"W. IAvH-P 10003 (1 c&s, 34.5 mm SL); Vichada, Cumaribo, caño Fruta, Orinoco River basin. 04°28'07.1"N 67°53'53.3"W. *Imparfinis pseudonemacheir*: IAvH-P 18648 (1 c&s, 29.3 mm SL); Casanare, Pore, río Pauto, 05°32'58.8"N 71°54'56.7"W, Orinoco River basin. IAvH-P 21974 (1 c&s, 23.7 mm SL); Arauca, Tame, morichal at El Vergel farm, Orinoco River basin, 06°16'51.2"N 71°42'49,0"W. *Leptorhamdia nocturna*: IAvH-P 6141 (1 c&s, 68.6 mm SL, Vichada); Cumaribo, río Tomo, Orinoco River basin, 05°22'46.4"N 68°3'33.2"W. *Mastiglanis asopos*: IAvH-P 13762 (1 c&s, 27.4 mm SL); Arauca, Cravo Norte, caño Juriepe, Orinoco River basin, 06°14'09.6"N 69°43'36.8"W. IAvH-P 16639 (1 c&s, 29.3 mm SL); Vichada, Puerto Carreño, caño Terecay, Orinoco River basin, 05°34'57.9"N 68°29'55.4"W. *Nemuroglanis mariae*: IAvH-P 16264 (1 c&s, 25.9 mm SL); Meta, La Macarena, NN stream, tributary of laguna El Silencio, Orinoco River basin, 02°14'57.5"N 73°45'33.8"W. IAvH-P 19640 (1 c&s, 32.7 mm SL), Meta, La Macarena, caño San José, Orinoco River basin, 02°33'01.2"N 73°56'27.2"W. *Nemuroglanis pauciradiatus:* IAvH-P 13763 (1 c&s, 20.7 mm SL); Arauca, Cravo Norte, caño Juriepe, Orinoco River basin, 06°14'09.6"N 69°43'36.8"W. IAvH-P 16930 (1 c&s 27 mm SL); Vichada, Puerto Carreño, caño Muñeco, Orinoco River basin, 05°35'12.8"N 68°29'07.4"W. *Phenacorhamdia anisura*: IAvH-P 7932 (1 c&s, 41 mm SL), Casanare, Aguazul, río Charte, Orinoco River basin, 05°15'27.9"N 72°29'14.9"W. IAvH-P 19767 (1 c&s, 56 mm SL); Meta, La Macarena, río Duda, Orinoco River basin, 02°32'56.5"N 73°57'12.9"W. IAvH-P 23826 (1 c&s, 33.5 mm SL); Meta, Castilla La Nueva, río Orotoy, Orinoco River basin, 03°51'13.5"N 73°27'03.11"W. *Pimelodella chaparae*: IAvH-P 20282 (1 c&s, 48.9 mm SL); Meta, Puerto Gaitán, río Manacacías, Orinoco River basin. *Pimelodella cruxenti*: IAvH-P 13900 (1 c&s, 66.2 mm SL); Arauca, Cravo Norte, caño Juriepe, Orinoco River basin, 06°13'58.1"N 69°42'57.3"W. *Pimelodella figueroai:* IAvH-P 22613 (1 c&s, 42.8 mm SL); Meta, La Macarena, caño Yarumales, Orinoco River basin, 02°23'30.9"N 73°35'24.6"W. *Pimelodella megalops*: IAvH-P 22612 (1 c&s, 35.6 mm SL); Meta, La Macarena, caño Yarumales, Orinoco River basin, 02°23'30.9"N 73°35'24.6"W. *Pimelodella* spp: IAvH-P 21322 (1 c&s, 57.1 mm SL); Meta, La Macarena, río Guayabero, Orinoco River basin, 02°17'33.6"N 73°52'39.6"W. IAvH-P 18858 (1 c&s, 79.1 mm SL); Casanare, Pore, río Pauto, Orinoco River basin, 05°32'58.8"N 71°54'56.7"W.

SUPPORTING INFORMATION

Supplementary data is available at *Zoological Journal of the Linnean Society* online.

Table S1. Catalog information of voucher specimens and BOLD accession numbers of sequences analyzed in DNA barcode species delimitation and phylogenomic analyses.

Figure S1. Species tree inference from Astral-III, based on the 70% complete matrix. No symbols at nodes indicate support values between 1–0.9, gray circles indicate nodal support between 0.89–0.75, and black circles indicate nodal support inferior to 0.75.

Figure S2. Best maximum likelihood tree based on the cytochrome c oxidase subunit I gene for Heptapteridae, based on available sequences in BOLD. Numbers near nodes indicate bootstrap support.

ACKNOWLEDGEMENTS

A.M.L., C.D., and J.G.A.G. thank the Instituto de Investigación de Recursos Biológicos Alexander von Humbolt for supporting the present study while the authors were affiliated with the Biological Collections division and more specifically with the Ichthyology Collection (IAvH-P). CD is indebted to Luz Fernanda Jiménez Segura and to Grupo de Ictiología of Universidad de Antioquia (GIUA) for supporting this research during affiliation of first author to Universidad de Antioquia. J. L. Londoño-López provided photographs of figures 3 and 8.

AUTHOR CONTRIBUTIONS

Conceptualization: C.C.C.S., C.D., F.A.V.N. Data curation: A.M.L., C.C.C.S., C.D., F.A.V.N., J.G.A.G. Formal analysis: C.C.C.S., C.D., F.A.V.N, F.F.R. Funding acquisition: C.D., F.A.V.N. Investigation: C.D., F.A.V.N. Methodology: A.O.L., C.C.C.S., C.D., F.A.V.N., J.G.A.G. Resources: A.O.L., C.O., G.C.S. Supervision: C.D. Validation: C.C.C.S., C.D. Visualization: A.M.L., C.C.C.S., J.G.A.G. Writing - original draft: C.C.C.S., C.D. Writing - review and editing: A.M.L., C.C.C.S., C.D., F.A.V.N., J.G.A.G., G.C.S., F.F.R., C.O.

CONFLICT OF INTEREST

The authors declare no conflicts of interest related to the present work.

FUNDING

C.C.C.S. was funded by the Sara E. and Bruce B. Collette Postdoctoral Fellowship in Systematic Ichthyology and by the Fundação de Amparo à Pesquisa do Estado de São Paulo grant #2018/09767-6. C.O. received financial support from Fundação de Amparo à Pesquisa do Estado de São Paulo - FAPESP grant 2020/13433-6, Conselho Nacional de Desenvolvimento Científico e Tecnológico - CNPq proc. 306054/2006-0 and 441128/2020-3, and Pro-Reitoria de Pesquisa da Universidade Estadual Paulista Júlio de Mesquita Filho (Prope-UNESP). G.C.S. was supported by FAPESP proc. 2021/12979-8.

DATA AVAILABILITY

To ensure the replicability of the present work, information of data matrix is summarized in Silva *et al.* (2021: supplementary table 1), and information on voucher specimens is presented in Supporting Information, Table S1. The 70% data matrix is available in Figshare (https://doi.org/10.6084/m9.figshare.28641899.v1).

REFERENCES

Aberer AJ, Kobert K, Stamatakis AE. ExaBayes: Massively parallel Bayesian tree inference for the whole-genome era. *Molecular Biology and Evolution* 2014;**10**:2553–6.

Albert JS, Lovejoy NR, Crampton WGR. Miocene tectonism and the separation of cis- and trans-Andean river basins: evidence from Neotropical fishes. *Journal of South American Earth Sciences* 2006;**1–2**:14–27.

Albornoz-Garzón JG, Conde-Saldaña CC, García-Melo JE *et al.* A new species of *Creagrutus* (Characidae: Stevardiinae) from the upper Río Magdalena, Colombia. *Zootaxa* 2018;**4482**:341–54.

Albornoz-Garzón JG, Conde-Saldaña CC, López-Delgado EO *et al.* Fishes from the Río Alvarado drainage, Upper Río Magdalena Basin, Colombia. *Check List* 2020;**16**:1181–98. https://doi.org/10.15560/16.5.1181

Alda F, Tagliacollo VA, Bernt MJ *et al.* Resolving deep nodes in an ancient radiation of Neotropical fishes in the presence of conflicting signals from incomplete lineage sorting. *Systematic Biology* 2019;**68**:573–93. https://doi.org/10.1093/sysbio/syy085

Ballen GA, Mojica JI. A new trans-Andean stick catfish of the genus *Farlowella* Eigenmann and Eigenmann, 1889 (Siluriformes: Loricariidae) with the first record of the genus for the río Magdalena Basin in Colombia. *Zootaxa* 2014;**3765**:134–42.

Betancur-R R, Wiley EO, Arratia G *et al.* Phylogenetic classification of bony fishes. *BMC Ecology and Evolution* 2017;**17**:1–40.

Bockmann FA. Description of *Mastiglanis asopos*, a new pimelodid catfish from northern Brazil, with comments on phylogenetic relationships inside the subfamily Rhamdiinae (Siluriformes: Pimelodidae). *Proceedings of the Biological Society of Washington* 1994;**4**:760–77.

Bockmann F. Análise filogenética da família Heptapteridae (Teleostei, Ostariophysi, Siluriformes) e redefenição de seus gêneros. Unpublished Ph.D. Thesis, Universidade de São Paulo, 1998.

Bockmann FA, Castro RMC. The blind catfish from the caves of Chapada Diamantina, Bahia, Brazil (Siluriformes: Heptapteridae): description, anatomy, phylogenetic relationships, natural history, and biogeography. *Neotropical Ichthyology* 2010;**8**:673–706. https://doi.org/10.1590/s1679-62252010000400001

Bockmann FA, de Pinna MCC. *Heptapterus collettii* Steindachner, 1881: a member of the Asian bagrid genus *Olyra* erroneously assigned to the Neotropical fauna (Siluriformes: Ostariophysi). *Copeia* 2004;**2004**:665–75. https://doi.org/10.1643/ci-03-198r1

Bockmann FA, Ferraris CJ. Systematics of the Neotropical catfish genera *Nemuroglanis* Eigenmann and Eigenmann 1889, *Imparales* Schultz 1944, and *Medemichthys* Dahl 1961 (Siluriformes: Heptapteridae). *Copeia* 2005;**2005**:124–37. https://doi.org/10.1643/ci-04-019r1

Bockmann F, Guazelli GM. Family Heptapteridae (Heptapterids). In: Reis RE, Kullander SO, Ferraris CJ (eds), *Check List of the Freshwater Fishes of South and Central America.* Porto Alegre: EDIPUCRS, 2003, 406–31.

Bockmann FA, Miquelarena AM. Anatomy and phylogenetic relationships of a new catfish species from northeastern Argentina with comments on the phylogenetic relationships of the genus *Rhamdella* Eigenmann and Eigenmann 1888 (Siluriformes, Heptapteridae). *Zootaxa* 2008;**1780**:1–54.

Bockmann FA, Reis RE. Two new, remarkably colored species of the Neotropical catfish genus *Cetopsorhamdia* Eigenmann & Fisher, 1916 (Siluriformes, Heptapteridae) from Chapada dos Parecis, western Brazil, with an assessment of the morphological characters bearing on their phylogenetic relationships. *Papéis Avulsos de Zoologia* 2021;**61**:e20216156–33. https://doi.org/10.11606/1807-0205/2021.61.56

Cassemiro FAS, Albert JS, Antonelli A *et al.* Landscape dynamics and diversification of the megadiverse South American freshwater fish fauna. *Proceedings of the National Academy of Sciences* 2023;**120**:e2211974120.

de Pinna MCC. Higher-level phylogeny of Siluriformes (Teleostei, Ostariophysi), with a new classification of the order. Unpublished Ph.D. Thesis, City University of New York, 1993.

Diogo R. *Morphological Evolution, Aptations, Homoplasies, Constraints and Evolutionary Trends: Catfishes as a Case Study on General Phylogeny and Macroevolution.* Enfield, NH: Science Publishers, 2005.

Diogo R. Osteology and myology of the cephalic region and pectoral girdle of *Heptapterus mustelinus*, comparison with other heptapterins, and discussion on the synapomorphies and phylogenetic relationships of the Heptapterinae and the Pimelodidae (Teleostei: Siluriformes). *International Journal of Morphology* 2007;**25**:735–48.

DoNascimiento C, Agudelo-Zamora HD, Bogotá-Gregory JD, *et al. Lista de especies de peces de agua dulce de Colombia / Checklist of the freshwater fishes of Colombia. v2.16. Asociación Colombiana de Ictiólogos. Dataset/Checklist.* 2023. https://doi.org/10.15472/numrso (June 2024, date last accessed).

Drummond AJ, Ho SYW, Phillips MJ *et al.* Relaxed phylogenetics and dating with confidence. *PLoS Biology* 2006;**4**:e88. https://doi.org/10.1371/journal.pbio.0040088

Drummond AJ, Suchard MA, Xie D *et al.* Bayesian phylogenetics with BEAUti and the BEAST 1.7. *Molecular Biology and Evolution* 2012;**29**:1969–73. https://doi.org/10.1093/molbev/mss075

Edgar RC. MUSCLE: Multiple sequence alignment with high accuracy and high throughput. *Nucleic Acids Research* 2004;**32**:1792–7. https://doi.org/10.1093/nar/gkh340

Esselstyn JA, Evans BJ, Sedlock JL *et al.* Single-locus species delimitation: a test of the mixed yule-coalescent model, with an empirical application to Philippine round-leaf bats. *Proceedings of the Royal Society B: Biological Sciences* 2012;**279**:3678–86. https://doi.org/10.1098/rspb.2012.0705

Faircloth BC, Alda F, Hoekzema K *et al.* A target enrichment bait set for studying relationships among ostariophysan fishes. *Copeia* 2020;**108**:47–60. https://doi.org/10.1643/cg-18-139

Faircloth BC. illumiprocessor: a trimmomatic wrapper for parallel adapter and quality trimming. *GitHub*. 2013. https://doi.org/10.6079/J9ILL

Faircloth BC. PHYLUCE is a software package for the analysis of conserved genomic loci. *Bioinformatics* 2016;**32**:786–8. https://doi.org/10.1093/bioinformatics/btv646

Faircloth BC, McCormack JE, Crawford NG *et al.* Ultraconserved elements anchor thousands of genetic markers spanning multiple evolutionary timescales. *Systematic Biology* 2012;**61**:717–26. https://doi.org/10.1093/sysbio/sys004

Faustino-Fuster DR, Meza-Vargas V, Lovejoy NR *et al.* Multi-locus phylogeny with dense Guiana Shield sampling supports new suprageneric classification of the Neotropical three-barbeled catfishes (Siluriformes: Heptapteridae). *Molecular Phylogenetics and Evolution* 2021;**162**:107186. https://doi.org/10.1016/j.ympev.2021.107186

Faustino-Fuster DR, Bockmann FA, Malabarba LR. Two new species of *Heptapterus* (Siluriformes: Heptapteridae) from the Uruguay River basin, Brazil. *Journal of Fish Biology* 2019;**94**:352–73. https://doi.org/10.1111/jfb.13908

Ferraris CJ. Relationships of the Neotropical catfish genus *Nemuroglanis*, with a description of a new species (Osteichthyes: Siluriformes: Pimelodidae). *Proceedings of the Biological Society of Washington* 1988;**3**:509–16.

Fricke R, Eschmeyer WN, Van der Laan R (eds). *Eschmeyer's Catalog of Fishes: Genera, Species, References.* 2024. http://researcharchive.calacademy.org/research/ichthyology/catalog/fishcatmain.asp (June 2024, date last accessed).

Fujisawa T, Barraclough TG. Delimiting species using single-locus data and the generalized mixed yule coalescent approach: a revised method and evaluation on simulated data sets. *Systematic Biology* 2013;**62**:707–24. https://doi.org/10.1093/sysbio/syt033

García-Alzate C, DoNascimiento C, Villa-Navarro FA *et al*. Diversidad de peces de la cuenca del río Magdalena, Colombia. In: Jiménez-Segura L, Lasso CA (eds), *Peces de la cuenca del río Magdalena, Colombia: Diversidad, conservación y uso sostenible.* Serie Editorial Recursos Hidrobiológicos y Pesqueros Continentales de Colombia. Bogotá, D.C.: Instituto de Investigación de Recursos Biológicos Alexander von Humboldt, 2020, 85–113.

Griffiths RC, Tavaré S. Sampling theory for neutral alleles in a varying environment. *Philosophical Transactions of the Royal Society B: Biological Sciences* 1994;**1310**:403–10.

Hardman M. The phylogenetic relationships among non-diplomystid catfishes as inferred from mitochondrial cytochrome *b* sequences; the search for the ictalurid sister taxon (Otophysi: Siluriformes). *Molecular Phylogenetics and Evolution* 2005;**37**:700–20. https://doi.org/10.1016/j.ympev.2005.04.029

Hardman M, Lundberg JG. Molecular phylogeny and a chronology of diversification for 'phractocephaline' catfishes (Siluriformes: Pimelodidae) based on mitochondrial DNA and nuclear recombination activating gene 2 sequences. *Molecular Phylogenetics and Evolution* 2006;**40**:410–8. https://doi.org/10.1016/j.ympev.2006.03.011

Hebert PDN, Cywinska A, Ball SL *et al*. Biological identifications through DNA barcodes. *Proceedings of the Royal Society B: Biological Sciences* 2003;**270**:313–21. https://doi.org/10.1098/rspb.2002.2218

Hendrich L, Pons J, Ribera I *et al*. Mitochondrial cox1 sequence data reliably uncover patterns of insect diversity but suffer from high lineage-idiosyncratic error rates. *PLoS One* 2010;**5**:e14448. https://doi.org/10.1371/journal.pone.0014448

Katoh K, Misawa K, Kuma KI *et al*. MAFFT: a novel method for rapid multiple sequence alignment based on fast Fourier transform. *Nucleic Acids Research* 2002;**14**:3059–66.

Kearse M, Moir R, Wilson A *et al*. Geneious basic: an integrated and extendable desktop software platform for the organization and analysis of sequence data. *Bioinformatics* 2012;**28**:1647–9. https://doi.org/10.1093/bioinformatics/bts199

Kumar S, Stecher G, Li M *et al*. MEGA X: molecular evolutionary genetics analysis across computing platforms. *Molecular Biology and Evolution* 2018;**35**:1547–9. https://doi.org/10.1093/molbev/msy096

Lanfear R, Calcott B, Ho SYW *et al*. PartitionFinder: combined selection of partitioning schemes and substitution models for phylogenetic analyses. *Molecular Biology and Evolution* 2012;**29**:1695–701. https://doi.org/10.1093/molbev/mss020

Lehmann AP, Usma Oviedo JS. *Genycharax tarpon* Eigenmann 1912. In: Mojica JI, Usma JS, Álvarez León R *et al*. (eds), *Libro rojo de peces dulceacuícolas de Colombia.* Bogotá, D.C.: Instituto de Investigación de Recursos Biológicos Alexander von Humboldt, Instituto de Ciencias Naturales de la Universidad Nacional de Colombia, WWF Colombia & Universidad de Manizales, 2012a, 118–9.

Lehmann AP, Usma Oviedo JS. *Astyanax aurocaudatus* Eigenmann 1913. In: Mojica JI, Usma JS, Álvarez León R, *et al*. (eds), *Libro rojo de peces dulceacuícolas de Colombia.* Bogotá, D.C.: Instituto de Investigación de Recursos Biológicos Alexander von Humboldt, Instituto de Ciencias Naturales de la Universidad Nacional de Colombia, WWF Colombia & Universidad de Manizales, 2012b, 199–200.

Londoño-Burbano A, Román-Valencia C, Taphorn DC. Taxonomic review of Colombian *Parodon* (Characiformes: Parodontidae), with descriptions of three new species. *Neotropical Ichthyology* 2011;**9**:709–30. https://doi.org/10.1590/s1679-62252011000400003

Londoño-Burbano A, Reis RE. A taxonomic revision of *Sturisomatichthys* Isbrücker and Nijssen, 1979 (Loricariidae: Loricariinae), with descriptions of three new species. *Copeia* 2019;**107**:764–806. doi:10.1643/CI-19-226

Lundberg JG, Baskin J. The caudal skeleton of the catfishes, Order Siluriformes. *American Museum Novitates* 1969;**2398**:1–49.

Lundberg JG, McDade LA. On the South American catfish *Brachyrhamdia imitator* Myers (Siluriformes, Pimelodidae), with phylogenetic evidence for a large intrafamilial lineage. *Notulae Naturae* 1986;**463**:1–24.

Lundberg JG, Bornbusch AH, Mago-Leccia F. *Gladioglanis conquistador* N. Sp. from Ecuador with diagnoses of the subfamilies Rhamdiinae Bleeker and Pseudopimelodinae N. Subf. (Siluriformes: Pimelodidae). *Copeia* 1991;**1991**:190–209. https://doi.org/10.2307/1446263

Lundberg JG, Marshall LC, Guerrero J *et al*. The stage for Neotropical fish diversification: a history of tropical South American rivers. In: Malabarba L, Reis RE, Vari RP *et al*. (eds), *Phylogeny and classification of Neotropical Fishes.* Porto Alegre: Museu de Ciências e Tecnologia, 1998, 13–48.

Maldonado-Ocampo JA, Villa-Navarro FA, Ortega-Lara A *et al*. Peces del río Atrato, zona hidrogeográfica del Caribe, Colombia. *Biota Colombiana* 2006;**7**:143–54.

Martínez JG, Rangel-Medrano JD, Yepes-Acevedo AJ *et al*. Species limits and introgression in *Pimelodus* from the Magdalena-Cauca River basin. *Molecular Phylogenetics and Evolution* 2022;**173**:107517. https://doi.org/10.1016/j.ympev.2022.107517

Miralles A, Vences M. New metrics for comparison of taxonomies reveal striking discrepancies among species delimitation methods in *Madascincus* lizards. *PLoS One* 2013;**8**:e68242. https://doi.org/10.1371/journal.pone.0068242

Mirande JM. Combined phylogeny of ray-finned fishes (Actinopterygii) and the use of morphological characters in large-scale analyses. *Cladistics* 2017;**4**:333–50.

Mo T. *Anatomy, Relationships and Systematics of the Bagridae (Teleostei: Siluroidei) with a Hypothesis of Siluroid Phylogeny.* Theses Zoologicae, 17. Köenigstein: Koeltz Scientific Books, 1991.

Montes C, Silva CA, Bayona GA *et al*. A Middle to Late Miocene Trans-Andean Portal: geologic record in the Tatacoa Desert. *Frontiers in Earth Science* 2021;**8**:587022.

Ochoa LE, Melo BF, García-Melo JE *et al*. Species delimitation reveals an underestimated diversity of Andean catfishes of the family Astroblepidae (Teleostei: Siluriformes). *Neotropical Ichthyology* 2020;**18**:e200048.

Ortega-Lara A, Usma JS, Bonilla PA *et al*. Peces de la cuenca alta del río Cauca, Colombia. *Biota Colombiana.* 2006;**1**:39–54.

Ortega-Lara A, Milani N, DoNascimiento C *et al*. Two new trans-Andean species of *Imparfinis* Eigenmann & Norris, 1900 (Siluriformes: Heptapteridae) from Colombia. *Neotropical Ichthyology* 2011;**9**:777–93. https://doi.org/10.1590/s1679-62252011000400009

Ortega-Lara A, Lasso-Alcalá OM, Lasso CA *et al*. Redescripción de *Cetopsorhamdia nasus* Eigenmann y Fisher, 1916 (Siluriformes: Heptapteridae). *Biota Colombiana* 2012;**13**:47–70.

Ortega-Lara A, Ospina V, Reyes MP *et al*. 2022. *Guía de campo para la identificación de los peces de la cuenca alta del río Cauca. Santiago de Cali, Corporación Autónoma Regional del Valle del Cauca - CVC & Fundación para la Investigación y el Desarrollo Sostenible - FUNINDES.* Valle del Cauca, Colombia: Alfagraphic E.U., 2022.

Pattengale ND, Alipour M, Bininda-Emonds ORP *et al*. How many bootstrap replicates are necessary? *Journal of Computational Biology* 2009;**17**:337–54. https://doi.org/10.1089/cmb.2009.0179

Paz A, Crawford AJ. Molecular-based rapid inventories of sympatric diversity: a comparison of DNA barcode clustering methods applied to geography-based vs clade-based sampling of amphibians. *Journal of Biosciences* 2012;**37**:887–96. https://doi.org/10.1007/s12038-012-9255-x

Pereira LHG, Hanner R, Foresti F *et al*. Can DNA barcoding accurately discriminate megadiverse Neotropical freshwater fish fauna? *BMC Genetics* 2013;**20**:1–14.

Poveda-Cuellar JL, Conde-Saldaña CC, Villa-Navarro FA *et al*. Phylogenetic revision of whisker-cheeked suckermouth catfishes (Loricariidae: *Lasiancistrus*) from east of the Andes: five species where once there were two. *Zoological Journal of the Linnean Society* 2023;**199**:688–712. https://doi.org/10.1093/zoolinnean/zlad042

Pugedo ML, de Andrade Neto FR, Pessali TC *et al*. Integrative taxonomy supports new candidate fish species in a poorly studied Neotropical region: the Jequitinhonha River Basin. *Genetica* 2016;**144**:341–9. https://doi.org/10.1007/s10709-016-9903-4

Rambaut A, Suchard MA, Xie D *et al*. *Tracer v1.6*. 2014. University of Edinburgh, Edinburgh, Scotland. http://tree.bio.ed.ac.uk/software/tracer/

Reis RE, Kullander SO, Ferraris CJ (eds). *Check List of the Freshwater Fishes of South and Central America*. Porto Alegre: EDIPUCRS, 2003.

Roxo FF, Ochoa LE, Sabaj MH *et al.* Phylogenomic reappraisal of the Neotropical catfish family Loricariidae (Teleostei: Siluriformes) using ultraconserved elements. *Molecular Phylogenetics and Evolution* 2019;**135**:148–65. https://doi.org/10.1016/j.ympev.2019.02.017

Sabaj MH. *Codes for Natural History Collections in Ichthyology and Herpetology (Online Supplement). v9.5*. Washington D.C.: American Society of Ichthyologists and Herpetologists, 2023. https://asih.org (November 2023, date last accessed).

Silfvergrip AMC. *A Systematic Revision of the Neotropical Catfish Genus Rhamdia (Teleostei, Pimelodidae)*. Stockholm: Stockholm University, Department of Zoology, Swedish Museum of Natural History, 1996.

Silva GSC, Roxo FF, Melo BF *et al.* Evolutionary history of Heptapteridae catfishes using ultraconserved elements (Teleostei, Siluriformes). *Zoologica Scripta* 2021;**50**:543–54. https://doi.org/10.1111/zsc.12493

Silva GSC, Rocha MS, Melo BF *et al.* Phylogenomics of the catfish family Pimelodidae with focus on the genus *Pimelodus* support the recognition of Sorubiminae and Pimelodinae (Teleostei, Siluriformes). *Zoologica Scripta* 2024;**53**:541–54. https://doi.org/10.1111/zsc.12671

Stamatakis A. RAxML version 8: a tool for phylogenetic analysis and post-analysis of large phylogenies. *Bioinformatics* 2014;**30**:1312–3. https://doi.org/10.1093/bioinformatics/btu033

Stewart DJ. A new pimelodid catfish from the deep-river channel of the Río Napo, eastern Ecuador (Pisces: Pimelodidae). *Proceedings of the Academy of Natural Sciences of Philadelphia* 1986;**1**:46–52.

Sullivan JP, Lundberg JG, Hardman M. A phylogenetic analysis of the major groups of catfishes (Teleostei: Siluriformes) using rag1 and rag2 nuclear gene sequences. *Molecular Phylogenetics and Evolution* 2006;**41**:636–62. https://doi.org/10.1016/j.ympev.2006.05.044

Sullivan JP, Muriel-Cunha J, Lundberg JG. Phylogenetic relationships and molecular dating of the major groups of catfishes of the Neotropical superfamily Pimelodoidea (Teleostei, Siluriformes). *Proceedings of the Academy of Natural Sciences of Philadelphia* 2013;**162**:89–110. https://doi.org/10.1635/053.162.0106

Talavera G, Dincă V, Vila R. Factors affecting species delimitations with the GMYC model: insights from a butterfly survey. *Methods in Ecology and Evolution* 2013;**4**:1101–10. https://doi.org/10.1111/2041-210x.12107

Tamura K, Nei M. Estimation of the number of nucleotide substitutions in the control region of mitochondrial DNA in humans and chimpanzees. *Molecular Biology and Evolution* 1993;**3**:512–26.

Taylor WR, van Dyke GC. Revised procedure for staining and clearing small fishes and other vertebrates for bone and cartilage study. *Cybium* 1985;**2**:107–19.

Torres-Mejía M, Hernández E, Senechal V. A new species of *Astyanacinus* (Characiformes: Characidae) from the Río Magdalena system, Colombia. *Copeia* 2012;**2012**:501–6. https://doi.org/10.1643/ci-10-160

Usma Oviedo JS, Ortega-Lara A. *Pimelodella macrocephala* (Miles 1943). In: Mojica JI, Usma JS, Álvarez León R *et al.* (eds), *Libro rojo de peces dulceacuícolas de Colombia*. Bogotá, D.C.: Instituto de Investigación de Recursos Biológicos Alexander von Humboldt, Instituto de Ciencias Naturales de la Universidad Nacional de Colombia, WWF Colombia & Universidad de Manizales, 2012, 136–8.

Vanegas-Ríos JA. Taxonomic review of the Neotropical genus *Gephyrocharax* Eigenmann, 1912 (Characiformes, Characidae, Stevardiinae). *Zootaxa* 2016;**4100**:1–92.

Villa-Navarro FA, Zuñiga-Upegui PT, Castro-Roa D *et al.* Peces del alto Magdalena, cuenca del río Magdalena, Colombia. *Biota Colombiana* 2006;**1**:3–22.

Villa-Navarro FA, Acero PA, Cala Cala P. Taxonomic review of Trans-Andean species of *Pimelodus* (Siluriformes: Pimelodidae), with the descriptions of two new species. *Zootaxa* 2017;**4299**:337–60.

Wade EJ, Hertach T, Gogala M *et al.* Molecular species delimitation methods recover most song-delimited cicada species in the European *Cicadetta montana* complex. *Journal of Evolutionary Biology* 2015;**28**:2318–36. https://doi.org/10.1111/jeb.12756

Ward RD, Zemlak TS, Innes BH *et al.* DNA barcoding Australia's fish species. *Philosophical Transactions of the Royal Society B: Biological Sciences* 2005;**360**:1847–57. https://doi.org/10.1098/rstb.2005.1716

Xia X. DAMBE7: new and improved tools for data analysis in molecular biology and evolution. *Molecular Biology and Evolution* 2018;**35**:1550–2. https://doi.org/10.1093/molbev/msy073

Zerbino DR, Birney EV. Algorithms for *de novo* short read assembly using de Bruijn graphs. *Genome Research* 2008;**5**:821–9.

Zhang J, Kapli P, Pavlidis P *et al.* A general species delimitation method with applications to phylogenetic placements. *Bioinformatics* 2013;**29**:2869–76. https://doi.org/10.1093/bioinformatics/btt499

Zhang C, Rabiee M, Sayyari E *et al.* ASTRAL-III: polynomial time species tree reconstruction from partially resolved gene trees. *BMC Bioinformatics* 2018;**19**:15–30.